INVESTIGATION OF GAS-PHASE METAL ION COMPLEXES USING INFRARED MULTIPLE PHOTON DISSOCIATION SPECTROSCOPY AND DENSITY FUNCTIONAL THEORY CALCULATIONS

A Thesis by

Ryan Patrick Dain

Bachelor of Arts, Wichita State University, 2006

Submitted to the Department of Chemistry

and the faculty of the Graduate School of

Wichita State University

in partial fulfillment of

the requirements for the degree of

Master of Science

May 2010

INVESTIGATION OF GAS-PHASE METAL ION COMPLEXES USING INFRARED MULTIPLE PHOTON DISSOCIATION SPECTROSCOPY AND DENSITY FUNCTIONAL THEORY CALCULATIONS

The following faculty members have examined the final copy of this thesis for form and content, and recommend that it be accepted in partial fulfillment of the requirement for the degree of Master of Science, with a major in Chemistry.

_____

Michael Van Stipdonk, Committee Chair

_____

David Eichhorn, Committee Member

_____

Douglas English, Committee Member

_____

James Bann, Committee Member

_____

Robert Owens, Committee Member

DEDICATION

To everyone I've taught and everyone who has taught me.

Because of you, I am me.

“And all this science I don’t understand/ it’s just my job five days a week”

-Elton John

“Schrödinger Was Right!”

-C.M. Leavitt

ACKNOWLEDGEMENTS

I would like to thank my parents, Pat and Ginger, for giving me everything I have and letting my mind grow unabated and my sister and brother, Rae Anna and Richard, for keeping me laughing no matter what. Thanks are also due to my advisor, Dr. Mike Van Stipdonk, for giving me a chance. I would also like to acknowledge the funding for my research via a grant from the U. S. National Science Foundation (NSF grant CAREER-0239800) and the Fairmount College of Liberal Arts and Sciences of Wichita State University. I would like to thank my committee members Paul Rillema, Doug English, David Eichhorn, Jim Bann and Robert Owens for everything that they taught me and for being a part of this process. My successful career at WSU has been made possible thanks to the following individuals: Chris Leavitt (the best drinking buddy a guy could have), Sam Molesworth, Sarah Young, Kelsey Witherspoon, Mike Kullman, Zack Parsons, Sandra Osburn, Dale Kerstetter, Justin Lygrisse, Jung Oh, Stephanie Curtice, Gary Groenewold, Jos Oomens, Jeff Steill, Bela Paiz, Benjamin Bythell, Big Head, Little Head, Evan Williams, Jim Beam, Jack Daniels, W.L. Weller, Ezra Brooks, Early Times, The Miller High Life Moon Girl, Old Ducks, Gene Stephenson, The Wichita Dance Mafia, Rocky Balboa, Stephen King and oh so many more.

ABSTRACT

A combination of theoretical chemistry and "action" spectroscopy has become the most used tool for the exploration of gas-phase molecular ions. In this study, density functional theory (DFT) calculations were used to test the validity of conclusions drawn from the results of a matrix-isolation infrared (MI-IR) experiment and develop a modeling method that could be used for metal-coordinating chlorate ion pairs. That modeling method was then used in comparison with experimental infrared multiple photon dissociation (IRMPD) spectroscopy to determine the structures of metal-chlorate anions. In addition to structural information, the effect of the modeling method on spectral correlation was also investigated.

TABLE OF CONTENTS

TABLE OF CONTENTS (Cont.)

LIST OF FIGURES

Figure Page

LIST OF TABLES

Table Page

CHAPTER 1

Introduction

1.1 General Information

Structure governs many of the intrinsic properties of a molecule such as polarity, reactivity, magnetism and biological importance. Therefore, it is vitally important to be able to accurately determine the structure of a species of interest. Many methods have been developed and implemented to help with the determination of molecular structure. Methods such as nuclear magnetic resonance (NMR) and infrared (IR) spectroscopy and X-ray crystallography have been used for decades to deduce the structures of molecules both old and new. With each method, however, comes limitations as well as strengths.

Organic molecules are perfectly suited for NMR, for example, due to the presence of magnetic nuclei in ^{1}H and ^{13}C atoms and their response to applied radio frequency (rf) energy in an external magnetic field. Drawbacks to NMR include inherent low sensitivity, and the fact that protic solvents, such as water or methanol, will interfere with spectral collection so non-protic solvents such as carbon tetrachloride or deuterated chloroform must be used. Solid-state NMR removes the limitations due to low solubility but introduces a new set unto itself, such as probe design, sampling efficiency and cost. [1]

X-ray crystallography, in use since the 1940s, works well for a wide range of different molecules, from small inorganic coordination compounds to large protein complexes. This method involves measurement of diffraction patterns of X-rays that pass through pure crystallized material. Correctly correlating the diffraction pattern with a molecular structure can be tricky and the problems only grow as the molecule increases in complexity. It can take years

of practice and study to become proficient in solving crystal structures. The biggest limitation, however, is in the crystal itself. A pure, well made crystal of sufficient size is required for sampling, which is often the rate limiting step in generating a crystal structure. [1]

One drawback shared by both methods is the influence of outside factors on the structure obtained. Structural information generated from traditional NMR spectroscopy can be influenced by the nature of the solvents and the other analyte molecules present in solution. In X-ray crystallography, the structure of the molecule can be affected by the crystallization process itself. To determine the intrinsic structure of a molecule, the effects of solvents and other molecules need to be removed. This can be accomplished by moving the system to be characterized into the gas-phase, an environment that is devoid of solvent by default. The most common way gas-phase chemistry is explored today is through the use of mass spectrometry.

In general, mass spectrometry relies on two different processes: creating gas-phase ions via an ionization source and using an outside magnetic or electric field to separate the ions based on their mass to charge (m/z) ratio. Some structural information can be garnered from mass spectrometry techniques, most often by examining the fragmentation of an ion of interest. Using the difference between the m/z of product ions and that of the molecular ion of interest one can determine the identity of the neutral fragment lost to generate the product ion. Certain structural features can be inferred by investigating fragmentation and applying chemical intuition. Beyond this, however, no direct structural information is provided that is analogous to, for example, NMR or infrared (IR) spectroscopy.

Infrared spectroscopy, in the traditional sense, is particularly challenging for molecular ions in a mass spectrometer. The inherently low densities of “absorbers” in most mass

spectrometers prevents measurement of either the absorption or transmission of IR light through an isolated ion cloud. One way around this problem is to isolate the generated ions into an inert matrix, known as matrix isolation infrared (MI-IR) spectroscopy. This has been used extensively to characterize the structure of gas-phase species in the past [2-12], but the drawbacks of ambiguous spectra and possible structural changes from the isolation process still remain an issue [13].

Infrared multiple photon dissociation (IRMPD) spectroscopy is an "action spectroscopy" process that relies on the rapid distribution of absorbed photon energy into a variety of background vibrational states. This process, known as intramolecular vibrational redistribution or IVR, allows the energy of each photon to be dissipated before the ion absorbs another, which leads to the promotion of ion internal energy toward the dissociation threshold via multiple photon absorption [15-17]. The high, eventual internal energy of the system leads to fragmentation of the molecular ion which can be measured if the entire process takes place in the mass analyzer of a mass spectrometer instrument. By monitoring fragmentation yields as a function of photon wavelength or frequency, an IR spectrum similar to a linear absorption spectrum can be produced.

Due to the high dissociation thresholds for many molecules, several eV in some cases, a high power laser is needed to conduct photodissociation experiments. CO_2 gas discharge laser have been in use since the 1970s to induce photofragmentation for IRMPD spectroscopy, but they offer little wavelength tunability. A free electron laser (FEL) can provide the wideband range and power needed to make IRMPD spectroscopy as useful as it possibly can be. The unbound electrons provide a unique lasing medium, with spectral range segments not normally

accessible with traditional lasers. The major drawback is their high cost, need for large electron accelerators and related instrumentation and scarcity in the world [18-20].

The Free Electron Laser for Infrared eXperiments (FELIX) facility at the FOM-Institute for Plasma Physics "Rijnhuizen" is one location that has a FEL source available and the necessary equipment to perform FEL-based IRMPD measurements. The FELIX FEL is coupled to a Fourier-transform ion cyclotron resonance (FT-ICR), ion trapping, mass spectrometer, which provides both high mass accuracy as well as mass resolution. The general set up for FELIX is shown in Figure 1.

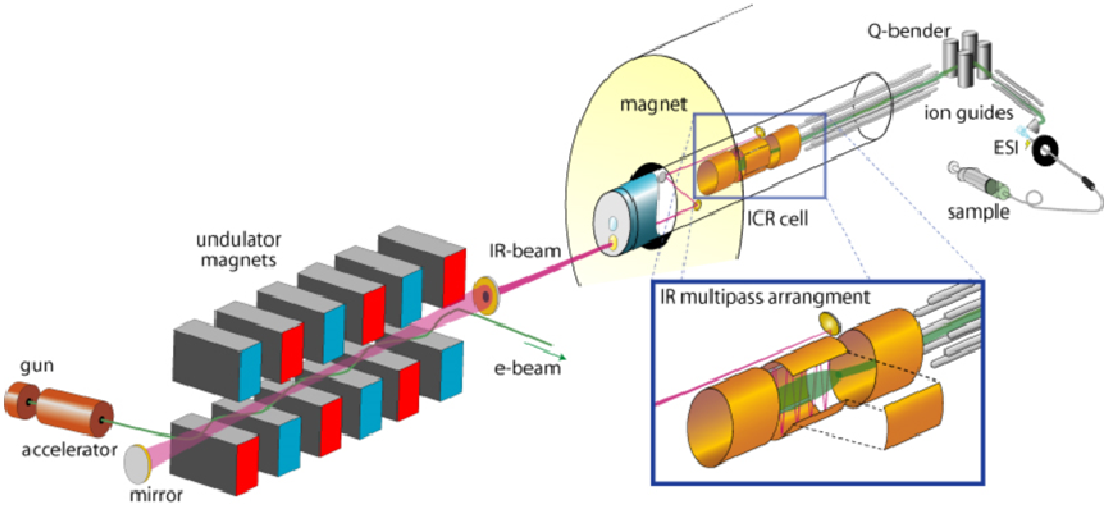

Figure 1: Free Electron Laser for Infrared eXperiments (FELIX)

The FEL has a continuous tunable wavelength range that is between 5 and 250 μm (200-40 cm^{-1}). Tunability is achieved by changing the distance between the magnets in the radio frequency linear accelerator (r.f. Linacs) region. The output consists of macropulses lasting between 5 to 10 μs, which can reach energies of 100 mJ with a maximum repetition rate of 10 Hz. Each macropulse is made of a rapid succession of micropulses which can be between 0.3 to 5 ps, with a separation time of 1 ns. The laser light is redirected through a series of optics from the basement, where the FEL is housed, to the FT-ICR lab. The laser beam is introduced into the

vacuum chamber under the ICR cell through a ZnSe window. A series of Cu mirrors generate a multipass region for the laser to pass through the ion population at the center of the ICR cell [23, 24]. The remaining parent ions and newly formed fragments are then excited and sent to the detector, where the photodissociation yield is measured as a function of wavelength and corrected for laser power. This produces an IR spectra that is comparable to one generated from a traditional, linear IR technique [25].

The generation of an IR spectrum for a discrete, gas-phase species is only the first half in the method to fully elucidate molecular structures. Quantum molecular modeling provides a theoretical optimized structure with an associated theoretical vibration spectrum that can be used to make final structural assignments, by correlating the experiment and theoretical spectral results. This is most often achieved through density functional theory (DFT) calculations. DFT calculations use quantum mechanics to model the electron densities in a molecule. The modeling of the electrons gives rise to the bonding nature of the atoms within the molecule, which in turn gives the optimized geometry. The nature of the calculation is governed by two different sets of parameters that change the way the calculation is handled. The first is the functional, which controls the way the total energy of the electrons is calculated, and the second is the basis set, which creates Slater-type orbitals from a linear combination of Gaussian-type orbitals. The most common functionals used, such as B3LYP and PBEPBE, are actually hybrid functionals. They borrow characteristics from Hartree-Fock (HF) and from other *ab initio* methods such as Local-Density Approximation (LDA). HF methods model the wavefunction of the electron, rather than the electron density. Each method has its merits and works well for certain types of systems, so choosing the correct functional is essential in getting the right answers for the right reasons.

Improving the performance of the basis set can be achieved by adding modifiers to the minimal basis sets. A minimal basis set, STO-nG where n represents the number of Gaussian primitive functions that make a single basis set function, can be improved upon by adding diffuse (d) and polarizing (p) functions. D functions are shallow Gaussian functions, which more accurately model the orbital as it gets farther from the atomic nuclei. P functions add nodes to the orbital, which is more realistic for the nature of bonding orbitals. In addition to added functions, using split valence basis sets can improve the accuracy of the calculation. It should be noted that each addition above and beyond the minimal basis set will increase the computational resources needed to complete the calculation. One way to handle electron heavy systems is to use a pseudopotential, which treats the inner core electrons as a single point charge and models only the valence electrons. This is very useful for modeling heavy atoms, which often do not have the basis set parameterization necessary to complete the calculations without pseudopotentials. It can take several calculations before the correct combination of functional and basis set can be found for a new system.

The overall aim of this thesis is to explore the structure of metal-containing, polyatomic complexes in the gas-phase through a combination of theoretical chemistry and IRMPD spectroscopy. In the first chapter of this thesis, a DFT modeling method was developed to make structural assignments using previously published MI-IR spectra for group 1 metal-chlorate ion pairs and their monohydrates. The work was completed as an attempt to fine tune the method needing for modeling the coordination of metal ions with oxygen-containing anions, taking special interest in the differing binding modes present and the effect of a coordinating water molecule on the molecular structure. The results showed that some of the structural assignments were most likely based on false assumptions and that new, more-likely structures were proposed,

backed up by the relative energies of the species and the correlation between the experimental and theoretical spectra.

In the second chapter of this thesis, the modeling method developed for the metal-chlorate ion pairs was tested on the metal-chlorate anionic dimers. For this work, the experimental spectra were generated with IRMPD spectroscopy using the FELIX facility. Spectra of sodium and potassium chlorate anions were gathered and compared to theoretical spectra generated by DFT to make structural determinations. In addition to determining the structure of these species, the modeling method was further examined by looking at the effect of functional and basis set on the general agreement of the experiment and theory. The results showed that the coordination mode of the anion was dependent on the cation and that the modeling method had a large effect on the position and splitting of the vibrational modes observed.

CHAPTER 2

Computational Investigation of Group 1 Metal-Chlorate Ion Pairs and Their Monohydrates

2.1 Introduction

The structures and bonding characteristics of metal-anion ion pairs have been the subject of a number of experimental and theoretical studies [2-12, 40, 41]. Experimental data for ion pairs such as metal nitrates, chlorates and perchlorates has been derived primarily from matrix isolation infrared absorption (MI-IR) investigations, and information extracted from such studies includes preferred coordination mode(s) by the respective anions (i.e. bidentate versus tridentate) and the effect of metal binding on characteristic anion absorption frequencies. For example, metal nitrate ion pairs have been studied because the vibrations of the nitrate anion are sensitive to chemical environment. The dominant feature in the infrared spectrum of alkali metal nitrates is the antisymmetric (ν_3) NO_3 stretch, which appears in the region of 1360 – 1400 cm^{-1}. However, for discrete metal nitrate ion pairs MI-IR experiments suggest that the cation distorts the D_{3h} symmetry of the anion, which in turn splits the degenerate ν_3(e) (NO_3^- antisymmetric stretching) mode into ν_{3a} and ν_{3b} components [2,3]. Within a limited number of systems, the magnitude of the splitting ($\Delta\nu_3$) has been shown to be proportional to the metal binding strength [2].

The subject of this chapter is group I metal-chlorate ion pairs, $M^+ClO_3^-$, which have been the target of prior experimental [4] and computational investigation [41-45], and the monohydrates of these species, $M^+ClO_3^-\bullet H_2O$. Throughout this thesis, the designation of composition as $M^+ClO_3^-$ or $M^+ClO_3^-\bullet H_2O$ is used to distinguish the isolated, contact ion pair from the compounds as bulk solids. Following an experimental study using MI-IR spectroscopy,

Ritzhaupt and Devlin [4] suggested that $Li^+ClO_3^-$ adopts a structure that features bidentate coordination of the metal ion by chlorate, while $Na^+ClO_3^-$ exists as a mixture of isomers with bidentate or tridentate coordination of the cation. By seeding the Ar matrix with H_2O, the structures of the monohydrates of the ion pairs ($M^+ClO_3^-•H_2O$) could be investigated. The bidentate coordination motif appeared to be retained for $Li^+ClO_3^-•H_2O$. However, for the $Na^+ClO_3^-$ ion pair addition of the H_2O ligand caused a shift in preference towards tridentate coordination of the cation by ClO_3^-. Discussion of the structures of the K^+ ion pair, bare and hydrated, was also included, with the suggestion that $K^+ClO_3^-$ exclusively adopts structures that feature tridentate coordination by chlorate within both the bare ion pair and the monohydrate.

Ramonado and coworkers used Hartree-Fock (HF) and Møller-Plesset (MP) ab-initio calculations (HF-SCF, MP2 and MP3) to determine the structures and harmonic frequencies for $Li^+ClO_3^-$ and $Na^+ClO_3^-$. Using HF-SCF calculations, the bidentate $Li^+ClO_3^-$ structure was found to be favored over the tridentate structure by approximately 24 kJ/mol (5.73 kcal/mol), while for $Na^+ClO_3^-$ the tridentate structure was favored by ca. 7 kJ/mol (1.67 kcal/mol) over the bidentate conformation. However, using MP2 and MP3 calculations, the bidentate structure was found to be favored for both $Li^+ClO_3^-$ and $Na^+ClO_3^-$ [45]. Solomonik and Pogrebnaya later eliminated some ambiguity by using HF and MP2 level calculations to investigate the potential structures of the bare (un-hydrated) Li^+, Na^+ and K^+-chlorate ion pairs. In their investigation, $Li^+ClO_3^-$ was predicted to favor a bidentate structure with C_s symmetry and $K^+ClO_3^-$ to preferentially adopt a tridentate conformation with C_{3v} symmetry. Both the bidentate and tridentate structures were found to be minima for the $Na^+ClO_3^-$, with an energy difference of ca. 0.4 kJ/mol (0.096 kcal/mol) between the two and a low interconversion barrier. Qualitatively, the conclusions

from the HF/MP2 study by Solomonik and Pogrebnaya were in agreement with suggested structures derived from the MI-IR experiments [41].

The scope of this work was to provide a comprehensive examination of the structures of $M^+ClO_3^-$ and $M^+ClO_3^-•H_2O$, where M=Li, Na, K, Rb and Cs, using density functional theory, which to date has not been used to model these specific systems. In the majority of our calculations we used the hybrid B3LYP functional and a range of basis sets with polarization and diffuse functions. One goal was to determine the relative energies of bidentate and tridentate ion-pair structures. Of greater interest, however, were the potential structures of the monohydrates, and their predicted infrared absorption frequencies, because these have not yet been the subject of a computational study. The structures and theoretical infrared spectra for both groups of species are presented for comparison to the experimental MI-IR benchmarks.

2.2 Computational Methods

All calculations were performed using the Gaussian 03 group of programs [44]. Initial geometries for all species were optimized with the B3LYP functional and the 6-31g(d) basis set on Li, Na, K, Cl and O. The MWB28 and MWB46 pseudopotentials and associated basis sets were used on Rb and Cs, respectively. To locate minima for the bare (un-hydrated) ion pairs, multiple independent calculations were begun by separating the metal cation and chlorate anion by > 4 Å, and allowing the two to approach during the optimization until a minimum was found. A similar approach was used to find the minima for the respective monohydrates.

For the Li, Na and K-containing species, the initial structures were re-optimized with the same functional and the 6-311+G(d), 6-311+G(2d) and 6-311+G(3df) basis sets for the bare ion pairs, and 6-311+G(d,p), 6-311+G(2d,p) and 6-311++G(3df,2pd) basis sets for the

monohydrates, except for those species in which the MBW28 and MBW46 pseudopotentials were used for the Rb and Cs cations, respectively. For most optimizations, a convergence criterion of 10^{-8} was used. In some cases, particularly for monohydrates for which one or more imaginary frequency was observed in the calculated infrared spectra, tighter optimization criteria were used.

The B3LYP functional and the 6-31 and 6-311-type basis sets were used for the bulk of our calculations because of their common use with similar systems, and because they have been used successfully by our group to predict infrared absorption features for discrete, gas-phase metal complexes [47-50]. As discussed below, the trends in our study with respect to the minima found and preferred structures are consistent with earlier HF and MP2 level calculations for $Li^+ClO_3^-$, $Na^+ClO_3^-$ and $K^+ClO_3^-$ by Solomonik and Pogrebnaya.

For $Na^+ClO_3^-$, a transition state for the conversion of the bidentate to the tridentate structure (vide infra) was found using the QST2 method. Because the transition state was a straightforward conversion and obvious from examination of the single negative frequency produced, intrinsic reaction coordinate calculations were not necessary or performed. Frequency calculations were performed using the B3LYP functional and the basis sets listed above, and used to provide zero-point energy corrections, establish global and local minima and for prediction of infrared absorption. For discussion below of ion-pair and hydrated ion-pair structures, data from species optimized with the 6-311+G(3df) and 6-311++G(3df,2dp) basis sets (or the MWB28 and MWB46 versions for Rb and Cs) are used, respectively.

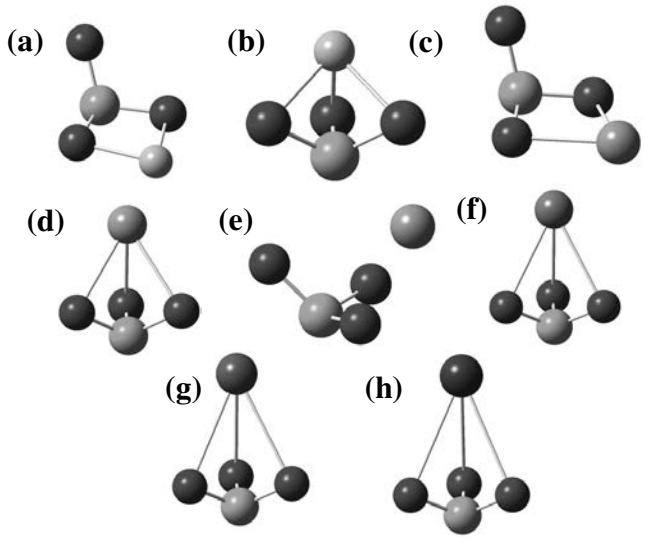

Figure 2: 6-311+G(3df) optimized structures of bare (a) bidentate $Li^+ClO_3^-$, (b) tridentate $Li^+ClO_3^-$, (c) bidentate $Na^+ClO_3^-$, (d) tridentate $Na^+ClO_3^-$, (e) bi- and tridentate $Na^+ClO_3^-$ transition state, (f) $K^+ClO_3^-$, (g) $Rb^+ClO_3^-$ and (h) $Cs^+ClO_3^-$ ion pairs

2.3 Results and Discussion

2.3.1 Structures of Group 1 Metal-Chlorate Ion Pairs

Figure 2 shows the structures found for the $Li^+ClO_3^-$ and $Na^+ClO_3^-$ ions pair using the B3LYP functional and the 6-311+G(3df) basis set. As with earlier computational studies and as suggested by the MI-IR investigations, $Li^+ClO_3^-$ species optimized to a structure that features bidentate coordination of the cation by the chlorate anion, while minima corresponding to bidentate and tridentate structures were identified for $Na^+ClO_3^-$. In general, the same minima for $Li^+ClO_3^-$ and $Na^+ClO_3^-$ were located regardless of the basis set used. No imaginary frequencies were observed in the calculated infrared spectrum for either $Na^+ClO_3^-$ isomer, indicating that both represent true minima and are stable structures. Bond length and bond angle data for $Li^+ClO_3^-$ are provided in Table 1. The bond lengths, angles and relative energies for the $Na^+ClO_3^-$ isomers and the transition state located for interconversion are found in Table 2.

In our calculations, a tridentate structure was located for $Li^+ClO_3^-$ only after freezing atomic coordinates. All other attempts to arrive at a minimum for tridentate coordination

resulted in a reversion back to the bidentate coordination mode. With zero-point correction, the relative energy of the tridentate structure (with geometry constraints) lies approximately 60 kcal/mol higher than the alternative bidentate structure, thus clearly establishing the preference of $Li^+ClO_3^-$ for the bidentate conformation.

Calculated Values	Group 1 Metal Cation
	Li
Bond Lengths (in Å)	
M-O_b	1.855
M-Cl	2.408
Cl-O_b	1.533
Cl-O_u	1.450
Bond Angles (in deg.)	
O_b-Cl-O_b	100.721
O_u-Cl-O_b	109.243
Cl-O_b-M	90.105
O_b-M-O_b	79.068
Energy (in a.u.)	
Uncorrected	-693.3790
ZPEC	0.0128
ZPE	-693.3662

Table 1: Bond length, bond angles and energies between the bidentate form of $Li^+ClO_3^-$

The MI-IR experiments [4], and the calculations by Solomonik and Pogrebnaya [41], suggest that both the bidentate and tridentate structures are stable isomers for $Na^+ClO_3^-$. In our investigation, at the B3LYP/6-311+G(3df) level of theory, the tridentate conformation was found to be lower in energy than the bidentate isomer by ~0.5 kcal/mol, consistent with the suggested presence of both isomers in the MI-IR experiments, and the low energy difference predicted by the earlier HF and MP2 calculations. Comparing the bond lengths within the bidentate structure, insertion of the larger sodium ion into $M^+ClO_3^-$ causes a marked lengthening of the metal-oxygen bond, from 1.855 in $Li^+ClO_3^-$ to 2.211 Å in $Na^+ClO_3^-$, as well as the bond between the Cl atom

and the terminal, non-coordinating O atom. The coordinating Cl-O bond length decreased, and the unbound oxygen-chlorine bond increased, by 0.011 Å.

The relative energies for the bidentate and tridentate ion pair structures were found to be dependent on the basis set used for calculations. As shown in Table 3, for $Na^+ClO_3^-$ the tridentate structure was favored for each basis set used, but the difference in energy ranged from 1.4703 kcal/mol for the 6-31+g(d) basis set to as low as 0.0188 kcal/mol for the 6-311+G(d) basis set. The difference in energy was comparable for the 6-311+G(2d) and 6-311+G(3df) basis sets (0.4600 and 0.5648 kcal/mol, respectively).

Calculated Values	**Conformation**		
	Bidentate	**T.S.**	**Tridentate**
	Bond Lengths (in Å)		
M-O_b	2.211	2.261	3.400
M-Cl	2.776	2.671	2.563
Cl-O_b	1.522	1.514	1.501
Cl-O_u	1.461	1.474	1.501
	Bond Angles (in deg.)		
O_b-Cl-O_b	103.448	103.940	105.236
O_u-Cl-O_b	108.341	106.958	105.226
Cl-O_b-M	94.244	87.722	78.561
O_b-M-O_b	65.421	63.668	59.603
	Energies		
Uncorrected (a.u.)	-848.1454	-848.1449	-848.1462
ZPEC (a.u.)	0.0116	0.0114	0.0114
ZPE (a.u.)	-848.1339	-848.1336	-848.1348
ΔE (kcal/mol)	+0.5648	+0.7530	0

Table 2: Comparisons of bond lengths, bond angles and energies for all three bare $Na^+ClO_3^-$ ion pairs

Bare Ion Pairs ΔE Values (in kcal/mol)				
Conformation	**6-31-G(d)**	**6-311+G(d)**	**6-311+G(2d)**	**6-311+G(3df)**
Bidentate	+1.4703	+0.0188	+0.4600	+0.5648
Tridentate	+0.0	+0.0	+0.0	+0.0

Table 3: ΔE values, in kcal/mol, for $Na^+ClO_3^-$ at the 6-31G(d), 6-311+G(d), 6-311+G(2d) and 6-311+G(3df) levels of theory

Figure 2 shows structures found for the K, Rb and Cs chlorate bare ion pairs at the B3LYP/6-311+g(3df), B3LYP/MWB28/6-311+g(3df) and B3LYP/MWB46/6-311+g(3df) level of theory, respectively. For each cation, the equilibrium structure featured the tridentate coordination mode: optimizations initiated using a bidentate precursor structure resulted in collapse to the tridentate form. Using geometry constraints, specifically, maintaining interaction between the metal cation and all 3 O atoms of the chlorate ligand, to lock ion pairs into the bidentate structure resulted in structures for which there was at least one imaginary frequency in the predicted infrared spectrum. The displacement vectors for the negative frequencies were consistent with the transition from the bidentate structure to the tridentate conformation of the ion pair.

Calculated Values	**Group 1 Metal Cation**		
	K	**Rb**	**Cs**
Bond Lengths (in Å)			
avg. M-O	2.710	2.910	3.078
M-Cl	2.917	3.133	3.320
avg. Cl-O	1.500	1.499	1.499
Bond Angles (in deg.)			
avg. O-Cl-O	105.905	106.270	106.497
avg. Cl-O-M	82.180	84.079	85.566
O-M-O	52.387	48.689	45.890
Energy (in a.u.)			
Uncorrected	-1285.7941	-709.9574	-706.0100
ZPEC	0.0111	0.0110	0.0109
ZPE	-1285.7830	-709.9464	-705.9991

Table 4: Comparisons of bond lengths, bond angles and energies for the tridentate $M^+ClO_3^-$, M=K, Rb, Cs

Adoption of only the tridentate structure by $K^+ClO_3^-$ is consistent with the prior MI-IR and HF/MP2 calculations. Our results show that the tridentate structure is also the preferred conformation of the larger Rb and Cs cation-chlorate ion pairs. Comparisons of bond lengths, bond angles and energies for the tridentate structures are presented in Table 4. As the size of the cation increases, from K to Rb and finally Cs, the distance of the metal to the chlorate ligand

increases as well, from 2.710 Å for K to 2.910 Å for Rb and 3.078 Å for Cs. The Cl-O bond lengths remain relatively unchanged. The O-Cl-O bond angle also increased slightly with the increase in cation size, from 105.90° to 106.27° to 106.50° for K, Rb and Cs, respectively.

2.3.2 Structures of Monohydrated Group1 Metal-Chlorate Ion Pairs

The primary interest was to determine the structure(s) of the $M^+ClO_3^-•H_2O$ species. Figure 3 shows structures for the monohydrates of $Li^+ClO_3^-$ and $Na^+ClO_3^-$ located at the B3LYP/6-311++G(3df,2pd) level of theory. For $Li^+ClO_3^-•H_2O$, two stable structures were identified. The first structure was the monohydrate of the bidentate ion pair structure in which the H_2O ligand coordinates the cation opposite to the chlorate anion. The second structure is a modified form of the hydrated bidentate conformation, in which the H_2O ligand bridges the cation and one O atom of the chlorate ligand: this structure is referred to hereafter as "curled bidentate." Because the tridentate structure was found to be ca. 60 kcal/mol higher in energy, optimization of a monohydrate of this species in which the H_2O ligand is bound to the cation and opposite to ClO_3^- was not pursued. At the B3LYP/6-311++G(3df,2pd) level of theory, the hydrated bidentate and curled bidentate structures were separated by only 0.565 kcal/mol in favor of the latter, suggesting that significant populations of both structures are likely. Comparison of bond lengths, angles and energies for bidentate species are presented in Table 5.

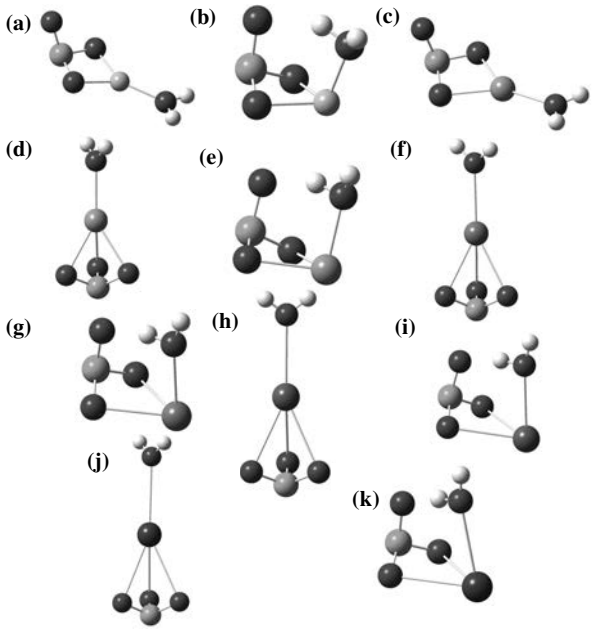

Figure 3: 6-311++G(3df, 2pd) optimized structures of monohydrated (a) bidentate $Li^+ClO_3^-$, (b) curled bidentate $Li^+ClO_3^-$, (c) bidentate $Na^+ClO_3^-$, (d) tridentate $Na^+ClO_3^-$, (e) curled bidentate $Na^+ClO_3^-$, (f) tridentate $K^+ClO_3^-$, (g) curled bidentate $K^+ClO_3^-$, (h) tridentate $Rb^+ClO_3^-$, (i) curled bidentate $Rb^+ClO_3^-$, (j) tridentate $Cs^+ClO_3^-$ and (k) curled bidentate $Cs^+ClO_3^-$ ion pairs

Three structures were identified for $Na^+ClO_3^-•H_2O$. Two correspond to conformations in which the H_2O ligand occupies a coordination site opposite ClO_3^- in the bidentate and tridentate structures. The third structure is the curled bidentate conformation in which the H_2O ligand bridges the Na^+ and ClO_3^-. For the hydrated tridentate structure, one imaginary frequency was observed in the predicted infrared spectrum, suggesting that the structure represents a saddle-point rather than a true minimum. The imaginary frequency remained when ultra fine integration was used. When tight optimization criteria were used, the hydrated tridentate structure collapsed to the curled bidentate structure. This strongly suggests the hydrated tridentate structure is not stable. With the caveat of the presence of a single imaginary frequency observed for the hydrated tridentate structure; with zero point correction the curled bidentate structure was favored energetically over the hydrated bidentate and hydrated tridentate conformations by 3.953 and 3.451 kcal/mol, respectively.

Calculated Values	Group 1 Metal Cation	
	Li	Na
Bond Lengths (in Å)		
M-H_2O	1.908	2.302
M-O_b	1.893	2.239
M-Cl	2.447	2.804
Cl-O_b	1.528	1.519
Cl-O_u	1.454	1.454
Bond Angles (in deg.)		
O_b-Cl-O_b	101.330	103.778
O_u-Cl-O_b	109.147	108.310
Cl-O_b-M	90.704	94.555
O_b-M-O_b	77.260	64.500
Energy (in a.u.)		
Uncorrected	-769.8720	-924.6312
ZPEC	0.0366	0.0346
ZPE	-769.8355	-924.5962

Table 5: Comparisons of bond length, bond angles and energies between the bidentate forms of $Li^+ClO_3^-$•H_2O and $Na^+ClO_3^-$•H_2O

As noted above for the bare ion pairs, the relative energies for the hydrated ion pair structures were dependent on the basis set used for calculations. Using $Na^+ClO_3^-$•H_2O as an example, the data shown in Table 6, shows that the hydrated bidentate structure for $Na^+ClO_3^-$ was predicted to be favored when the 6-31+G(d) basis set was used, with the hydrated tridentate and curled bidentate higher in energy by 23.3095 and 17.2584 kcal/mol, respectively. The curled bidentate structure was favored when the 6-311+G(d,p), 6-311+G(2d,p) and 6-311++G(3df,2pd) basis sets were used. Using 6-311+G(d,p), the relative energies for the hydrated bidentate and hydrated tridentate structures were comparable, while the hydrated bidentate structure was highest in energy when the two largest basis sets were used. As discussed below, the large 6-311++G(3df,2pd) appears to be most accurate for these species based on comparison between calculated (unscaled) and experimentally determined positions for chlorate stretches.

Monohydrates ΔE Values (in kcal/mol)				
Conformation	**6-31G(d)**	**6-311+G(d,p)**	**6-311+G(2d,p)**	**6-311++G(3df,2pd)**
Bidentate	+0.0	+4.1642	+3.5919	+3.9533
Tridentate	+23.3095	+4.2451	+3.2756	+3.4513
Curled Bidentate	+17.2584	+0.0	+0.0	+0.0

Table 6: ΔE values, in kcal/mol, for $Na^+ClO_3^-•H_2O$ at the 6-31G(d), 6-311+G(d,p), 6-311+G(2d,p) and 6-311++G(3df, 2pd) level of theory

For the K, Rb and Cs ion pairs, the two possible structures identified for $M^+ClO_3^-•H_2O$ were the hydrated tridentate structure, with H_2O ligand bound to the cation opposite ClO_3^-, and the curled bidentate structure. As for $Na^+ClO_3^-•H_2O$, a single negative frequency was observed the hydrated tridentate structures for $K^+ClO_3^-•H_2O$, $Rb^+ClO_3^-•H_2O$ and $Cs^+ClO_3^-•H_2O$, and each conformation collapsed to curled bidentate with use of tight convergence criteria. Because discussion of the hydrated tridentate structure is important to the interpretation of the MI-IR spectra of the hydrated ion pairs, the bond lengths, angles and energies for the tridentate species are presented in Table 7 and the relative energies of all species are included in Table 8. With zero-point energy correction, the curled bidentate structure was favored over the hydrated tridentate structure by 5.208, 5.146 and 5.648 kcal/mol, respectively, for $K^+ClO_3^-•H_2O$, $Rb^+ClO_3^-•H_2O$ and $Cs^+ClO_3^-•H_2O$. Thus for all $M^+ClO_3^-•H_2O$ species investigated, our calculations suggest that the $M^+ClO_3^-•H_2O$ species adopts the curled bidentate structure, which likely owes its stability to the formation of a hydrogen bonding interaction between the H_2O ligand and the chlorate anion. Comparison for the bond length, angles and energies for all curled bidentate species are presented in Table 9

.

Calculated Values	Group 1 Metal Cation			
	Na	**K**	**Rb**	**Cs**
Bond Lengths (in Å)				
M-H_2O	2.299	2.767	2.998	3.255
avg. M-O	2.423	2.744	2.940	3.110
M-Cl	2.591	2.947	3.136	3.349
avg. Cl-O	1.499	1.500	1.499	1.499
Bond Angles (in deg.)				
avg. O-Cl-O	105.421	106.104	106.430	106.585
avg. Cl-O-M	78.784	82.370	84.200	85.687
O-M-O	58.983	51.830	48.200	45.497
Energy (in a.u.)				
Uncorrected	-924.6316	-1362.2718	-786.4337	-782.4951
ZPEC	0.0346	0.0349	0.0338	0.0335
ZPE	-924.5970	-1362.2379	-786.3999	-782.4506

Table 7: Comparisons for bond lengths, bond angles and energies for the tridentate $M^+ClO_3^-•H_2O$, M=Na, K, Rb, Cs

Cation Conformations	ZPEC (a.u.)	ΔE (kcal/mol)
Li		
Bidentate	-769.8355	0
Curled Bidentate	-769.8346	+0.5648
Na		
Bidentate	-924.5962	+3.9533
Tridentate	-924.5970	+3.4513
Curled Bidentate	-924.6025	0
K		
Tridentate	-1362.2379	+5.2083
Curled Bidentate	-1362.2462	0
Rb		
Tridentate	-786.3999	+5.1456
Curled Bidentate	-786.4081	0
Cs		
Tridentate	-782.4506	+5.6476
Curled Bidentate	-782.4596	0

Table 8: Zero-point energy and ΔE values for $M^+ClO_3^-•H_2O$, M=Li, Na, K, Rb, Cs

Calculated Values	Group 1 Metal Cation				
	Li	**Na**	**K**	**Rb**	**Cs**
Bond Lengths (in Å)					
M-H_2O	1.916	2.302	2.603	2.811	2.992
M-O_b	1.982	2.323	2.658	2.869	3.041
M-Cl	2.437	2.780	3.158	3.356	3.545
Cl-O_b	1.514	1.506	1.502	1.499	1.498
Cl-O_u	1.482	1.490	1.494	1.497	1.498
O_u-H	1.980	1.852	1.804	1.786	1.777
Bond Angles (in deg.)					
O_b-Cl-O_b	102.323	104.498	105.584	106.206	106.416
O_u-Cl-O_b	107.422	107.400	107.301	107.306	107.328
Cl-O_b-M	87.340	90.650	94.670	95.262	96.779
O_b-M-O_b	73.017	61.836	53.504	49.397	46.473
Cl-M-H_2O	96.446	84.890	74.803	71.798	67.917
Energy (in a.u.)					
Uncorrected	-769.8723	-924.6388	-1362.2818	-786.4436	-782.4951
ZPEC	0.0378	0.0363	0.0356	0.0355	0.0354
ZPE	-769.8346	-924.6025	-1362.2462	-786.4081	-782.4596

Table 9: Comparisons for bond lengths, bond angles and energies for the curled bidentate $M^+ClO_3^-•H_2O$, M=Li, Na, K, Rb, Cs

2.3.4 Predicted IR Frequencies

Stretching frequencies predicted using DFT for the bare ion pairs, and the hydrated ion pairs, are provided in Tables 10 and 11. As suggested above, based on our DFT calculations the curled bidentate structure is the likely, if not preferred structure for the $M^+ClO_3^-•H_2O$ species, except for the Li species, for which both the hydrated bidentate and curled bidentate isomers are favored. In their earlier study, Ritzhaupt and Devlin suggested that $M^+ClO_3^-•H_2O$, where M^+ = Na^+ or K^+ will adopt the hydrated tridentate structure shown above regardless of the initial geometry of the bare ion pair [4]. As noted earlier, the DFT calculations performed in our study suggest that the hydrated tridentate structure is not stable. While the new, curled bidentate structure identified in the present study is not the standard planar bidentate structure of the

$M^+ClO_3^-$ species, we suggest that it should still technically be considered a bidentate structure because the cation is coordinated by only 2 O atoms of the chlorate anion.

Cation Conformation	Vibrational Frequency (cm^{-1})	Assignment
Li Bidentate	862	ν_{3b}
	877	ν_1
	1122	ν_{3a}
Na Bidentate	887	ν_{3b}
	893	ν_1
	1080	ν_{3a}
Na Tridentate	924	ν_1
	963	ν_3
	965	ν_3
K Tridentate	927	ν_1
	961	ν_3
	962	ν_3
Rb Tridentate	929	ν_1
	967	ν_3
Cs Tridentate	930	ν_1
	967	ν_3

Table 10: Vibrational stretching frequencies and assignments for $M^+ClO_3^-$, M=Li, Na, K, Rb, Cs

Cation Conformations	Vibrational Stretching Frequencies (cm^{-1})	Assignment
Li		
Bidentate	879	ν_{3b}
	887	ν_1
	1106	ν_{3a}
Curled Bidentate	913	ν_1
	921	ν_{3b}
	1014	ν_{3a}
Na		
Bidentate	898	ν_{3b}
	900	ν_1
	1070	ν_{3a}
Curled Bidentate	924	ν_1
	944	ν_{3b}
	989	ν_{3a}
Tridentate	927	ν_1
	966	ν_3
	968	ν_3
K		
Tridentate	928	ν_1
	962	ν_3
	963	ν_3
Curled Bidentate	931	ν_1
	955	ν_{3b}
	977	ν_{3a}
Rb		
Tridentate	929	ν_1
	968	ν_3
	969	ν_3
Curled Bidentate	935	ν_1
	968	ν_{3b}
	971	ν_{3a}
Cs		
Tridentate	930	ν_1
	967	ν_3
	968	ν_3
Curled Bidentate	935	ν_1
	969	ν_{3b}
	970	ν_{3a}

Table 11: Vibrational stretching frequencies and assignments for $M^+ClO_3^-\bullet H_2O$, M=Li, Na, K, Rb, Cs

The predicted IR spectra for $Li^+ClO_3^-\bullet H_2O$ and $Na^+ClO_3^-\bullet H_2O$ generated at the B3LYP/6-311++G(3df,2pd) level of theory are shown in figure 4a and 4b, respectively. The spectra are

shown unscaled, and were derived from the DFT calculations using a step size of 4 cm^{-1}. For $Li^+ClO_3^-•H_2O$ (figure 3a), both the hydrated bidentate and curled bidentate structures show two prominent absorption peaks, which we attribute to the ν_3 antisymmetric ClO_3^- stretch. The splitting of the ν_3 absorption is due to distortion of the anion symmetry due to interactions with the cation or the cation and water molecule. For the hydrated bidentate structure, the higher frequency ν_{3a} corresponds to the terminal (unbound) oxygen-chlorine stretch (O_u-Cl), while the lower frequency ν_{3b} absorption is assigned to the bound oxygen-chlorine stretch (O_b-Cl). For the curled bidentate structure, the position of the ν_{3a} stretch is affected by the hydrogen bonding interaction with the H_2O molecule. Ritzhaupt and Devlin reported an 18% reduction in the degeneracy splitting of the ν_3 mode, corresponding to decrease of 39 cm^{-1}, upon hydration of the bidentate form. For the hydrated bidentate structure of $Li^+ClO_3^-•H_2O$, the predicted IR spectra showed a 13% reduction in the degeneracy, corresponding to a decrease of 33 cm^{-1}. It is not clear whether an IR signature for the curled bidentate form of $Li^+ClO_3^-•H_2O$ was detected. Based on the DFT results, for this structure the degeneracy splitting, relative to the bare $Li^+ClO_3^-$ ion pair, was 93 cm^{-1}.

The ν_{3a} and ν_{3b} absorptions are also apparent in the IR spectra predicted for the hydrated bidentate and curled bidentate structures predicted for $Na^+ClO_3^-•H_2O$ (figure 3b). The IR spectrum for the hydrated tridentate structure features a dominant peak at ca. 965 cm^{-1}, which corresponds to the antisymmetric ClO_3^- stretch. Ritzhaupt and Devlin reported that the hydration of the $Na^+ClO_3^-$ contributed a single absorbance pattern of a doublet at 994 and 952 cm^{-1}, corresponding to the ν_3 mode, and a singlet at 927 cm^{-1}, corresponding to the ν_1 mode. The

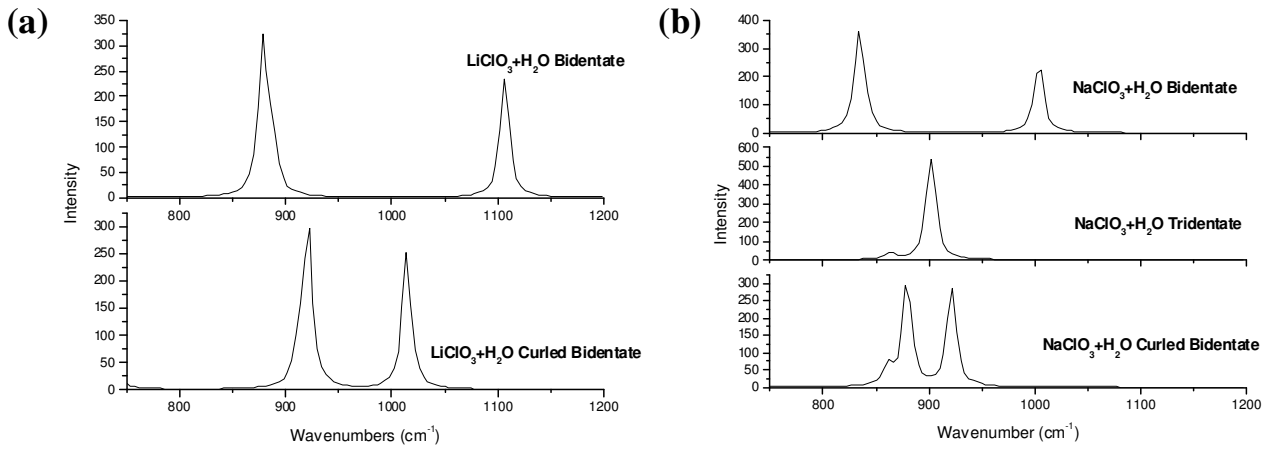

Figure 4: Predicted IR spectra comparisons for (a) $Li^+ClO_3^-•H_2O$ and (b) $Na^+ClO_3^-•H_2O$

splitting of the ν_3 mode, equal to 42 cm^{-1}, is attributed to a slight distortion of the tridentate structure [4]. The predicted IR spectrum of the curled bidentate $Na^+ClO_3^-•H_2O$ contains a similar splitting pattern of the ν_3 mode, equal to 45 cm^{-1}.

The predicted IR spectra for $K^+ClO_3^-•H_2O$, $Rb^+ClO_3^-•H_2O$ and $Cs^+ClO_3^-•H_2O$ are shown in Figure 5. The spectrum for $K^+ClO_3^-•H_2O$ (figure 5a) were generated at the B3LYP/6-311++G(3df,2pd) level of theory. The spectra for $Rb^+ClO_3^-•H_2O$ and $Cs^+ClO_3^-•H_2O$ (5b and 5c, respectively) were instead generated at the B3LYP/MWB28/6-311++G(3df,2pd) and B3LYP/MWB46/6-311++G(3df,2pd) level of theory, respectively. Despite the fact that the hydrated tridentate structure for the K^+, Rb^+ and Cs^+ ion pairs was found in our calculations to be unstable, the predicted spectra for the species is included in figure 5 because this conformation was proposed for $K^+ClO_3^-•H_2O$ based on the MI-IR experiments. As is apparent in figure 5a, both the ν_{3a} and ν_{3b} peaks appear in the spectrum predicted for $K^+ClO_3^-•H_2O$. However, the magnitude of the splitting of ν_3 is diminished considerably compared to the absorption pattern for $Li^+ClO_3^-•H_2O$ and $Na^+ClO_3^-•H_2O$. In addition, the relative positions of the absorptions

predicted for the hydrated tridentate and curled bidentate structures of $K^+ClO_3^-•H_2O$ are nearly identical. The previous MI-IR experiments suggest that the splitting of the ν_3 mode for $K^+ClO_3^-•H_2O$ is 23 cm^{-1}, and the IR spectrum from the present DFT calculation predicts a splitting of 22 cm^{-1} for the curled bidentate structure of $K^+ClO_3^-•H_2O$. The coalescence of the ν_{3a} and ν_{3b} absorptions is even more dramatic for $Rb^+ClO_3^-•H_2O$ and $Cs^+ClO_3^-•H_2O$ (figures 5b and 5c, respectively) in which the predicted IR spectra for the hydrated tridentate and curled bidentate structures are essentially identical.

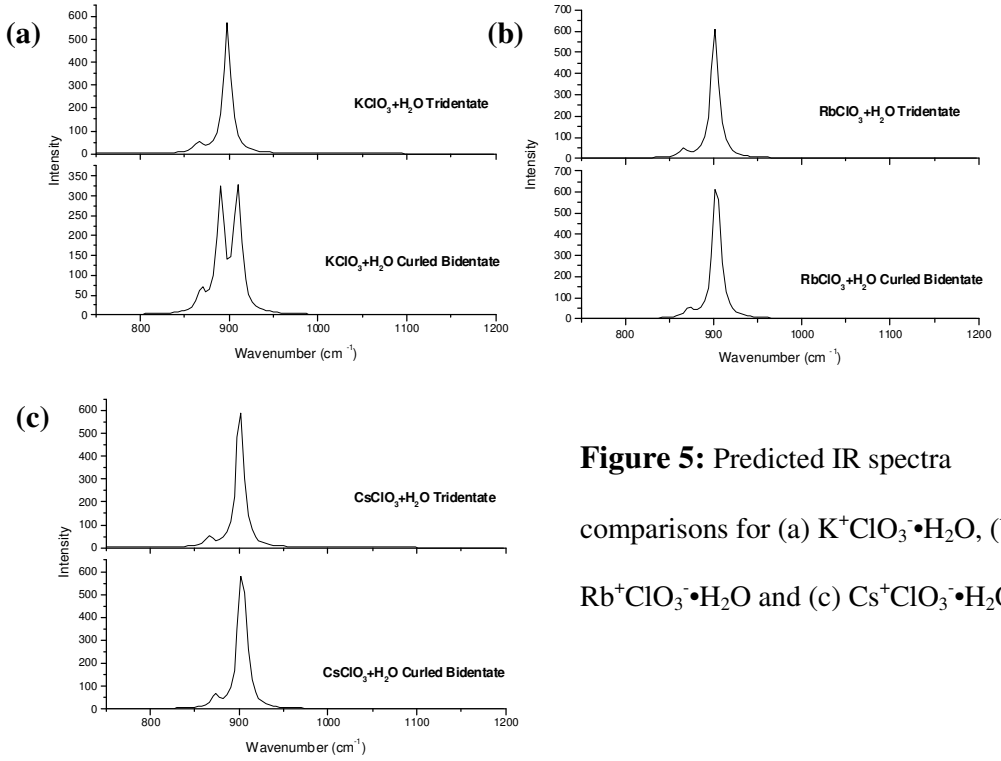

Figure 5: Predicted IR spectra comparisons for (a) $K^+ClO_3^-•H_2O$, (b) $Rb^+ClO_3^-•H_2O$ and (c) $Cs^+ClO_3^-•H_2O$

2.4 Conclusions

The structures and predicted infrared (IR) spectra of $M^+ClO_3^-$ and $M^+ClO_3^-•H_2O$, where M = Li, Na, K, Rb, Cs have been investigated using density functional theory calculations. The structures identified in this study for the $Li^+ClO_3^-$, $Na^+ClO_3^-$ and $K^+ClO_3^-$ contact ion pairs are in

good general agreement with earlier experimental and theoretical investigations, notably bidentate binding of Li^+ by chlorate in the $Li^+ClO_3^-$ ion pair, two isomeric structures for $Na^+ClO_3^-$ ion pair and the preferred tridentate binding of K^+ by chlorate in $K^+ClO_3^-$. In our study, the calculations were extended to include the Rb^+ and Cs^+ ion pairs: our modeling suggests that both $Rb^+ClO_3^-$ and $Cs^+ClO_3^-$ preferentially adopt the tridentate structure.

For the $M^+ClO_3^-•H_2O$ our calculations yielded multiple possible structures. While $Li^+ClO_3^-•H_2O$ and $Na^+ClO_3^-•H_2O$ both appear to form stable hydrated bidentate structures, the curled bidentate structure with a "bridging" H_2O ligand represents the global minimum for the hydrated ion pairs. For no hydrated ion pairs were we able to find a stable, hydrated tridentate structure. With respect to previous MI-IR studies, our calculations, and in particular, the predicted IR patterns for the lowest energy conformations of $Li^+ClO_3^-•H_2O$ and $Na^+ClO_3^-•H_2O$ are consistent with the MI-IR data. The spectra for the curled bidentate structures of $K^+ClO_3^-•H_2O$, $Rb^+ClO_3^-•H_2O$ and $Cs^+ClO_3^-•H_2O$ are sufficiently similar, if not identical to, those for a hydrated tridentate structure, it is likely that the two might not be distinguished in the experimental spectrum. As noted above, because the hydrated tridentate structure was not found to be a true minimum, we favor assignment of the actual structure to the curled bidentate.

Despite good qualitative agreement with the MI-IR benchmarks for $Li^+ClO_3^-•H_2O$ and $Na^+ClO_3^-•H_2O$, the overall accuracy of the present DFT calculations and in particular the positions of the expected absorptions is difficult to assess. Figures 6 and 7 show the predicted IR spectra for the curled bidentate structures of $Na^+ClO_3^-•H_2O$ and $K^+ClO_3^-•H_2O$, with the positions of the respective chlorate stretches (ν_1, ν_{3b} and ν_{3a}) as determined using MI-IR. Using the B3LYP functional and 6-311++G(3df,2pd) basis set, the unscaled predicted frequencies lie between 3 and 12 cm^{-1} to the red of the experimental values. The calculations performed in this

study are a prelude to further experiments that will involve the collection of infrared spectra for discrete metal-chlorate anions using wave-length selective infrared multiple-photon photodissociation (IRMPD). The IRMPD data will allow for further assessment of accuracy, and in particular, any scaling factors necessary to converge theory and experiment.

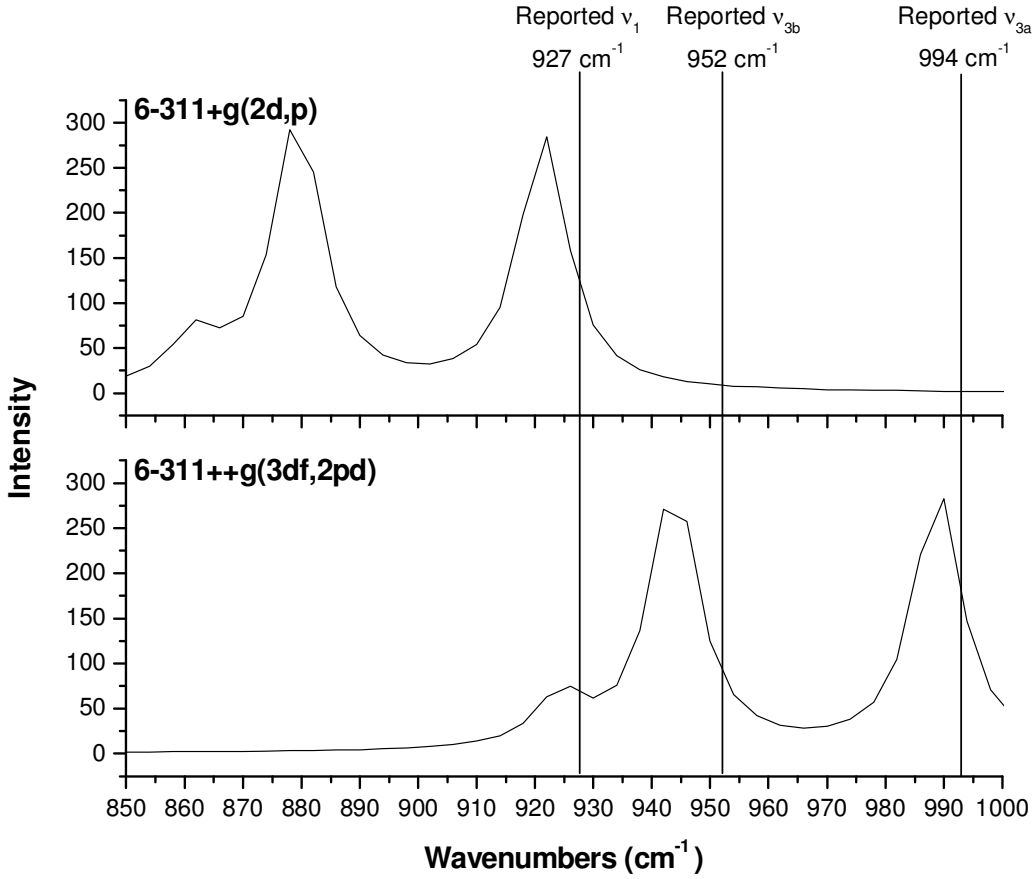

Figure 6: Comparison of absorbance placement in predicted IR spectra for curled bidentate conformation of $Na^+ClO_3^-•H_2O$ at the 6-311+G(2d,p) and 6-311++G(3df, 2pd) level of theory along with reported ν_1, ν_{3b} and ν_{3a} values.

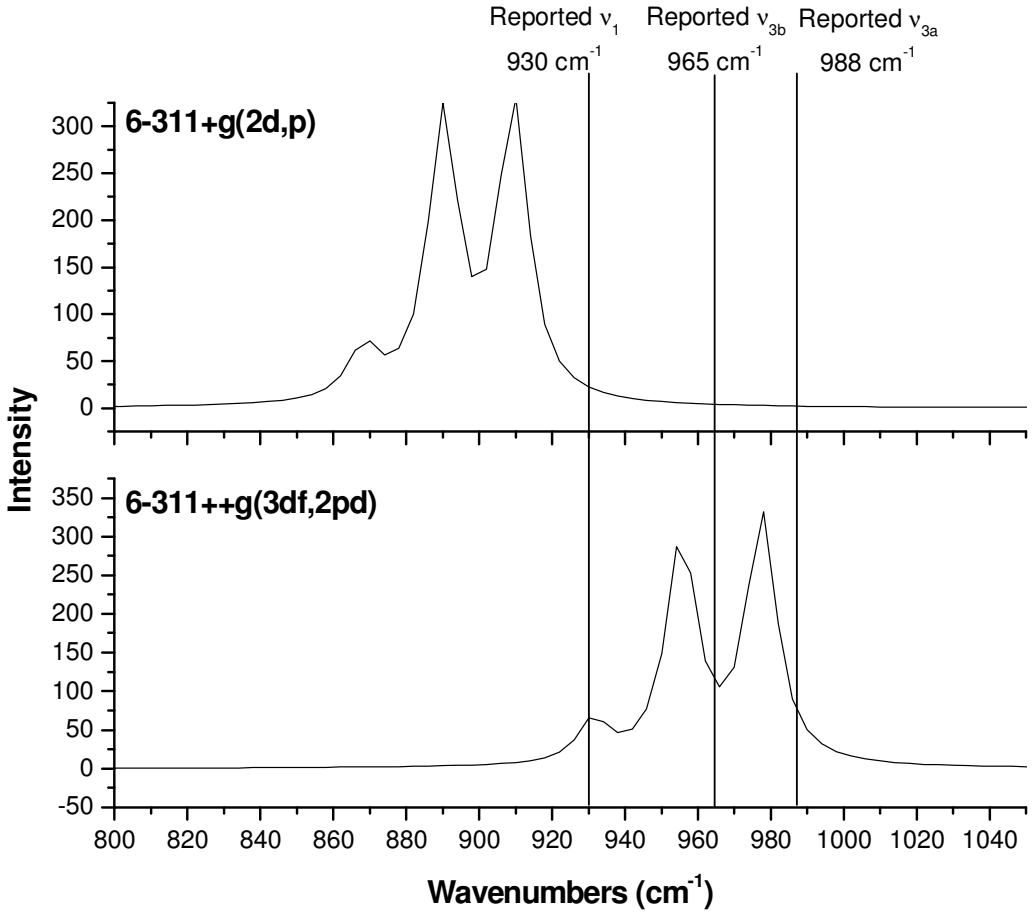

Figure 7: Comparison of absorbance placement in predicted IR spectra for curled bidentate conformation of $K^+ClO_3^-•H_2O$ at the 6-311+G(2d,p) and 6-311++G(3df, 2pd) level of theory along with reported ν_1, ν_{3b} and ν_{3a} values.

CHAPTER 3

IRMPD Spectroscopy of Sodium and Potassium Chlorate Anions

3.1 Introduction

In the previous chapter, DFT calculations were used to predict the structures of the group I metal-chlorate ion pairs, $[M^+ClO_3^-]$, and their monohydrates, $[M^+ClO_3^-\bullet H_2O]$, for comparison to previously published experimental (MI-IR) and theoretical (Hartree-Fock, HF and Moller-Plesset, MP) investigations [4, 41-44]. This particular system is of interest because the chlorate anion functions as either a bidentate or tridentate ligand depending on the metal cation. Optimized structures for the bare ion pairs predicted in our DFT study were in general agreement with MI-IR data [4] as well as previous HF/MP2 calculations, suggesting a mix of bidentate and tridentate coordination of Na^+ by chlorate, and exclusively tridentate coordination of K^+. However, for the monohydrates of the ion pairs, our study revealed a new, oxygen bridging "curled bidentate" structure, which is the lowest energy structure and, for sodium and potassium, provided the best agreement among the predicted IR spectra and the existing MI-IR benchmarks [4].

In the current chapter, the initial investigation of metal-chlorate species is extended to include anionic species with general formula $[M(ClO_3)_2]^-$, where $M=Na^+$ and K^+. The anions were generated by electrospray ionization (ESI) and their infrared spectra collected using a combination of tandem mass spectrometry and wavelength-selective infrared multiple-photon dissociation (IRMPD). The approach produces infrared spectra of discrete, gas-phase ions that are comparable to linear absorption spectra. In these experiments, our aim was to identify the intrinsic chlorate binding mode for both $[Na(ClO_3)_2]^-$ and $[K(ClO_3)_2]^-$. In addition, the gas-phase

IR measurements provide benchmarks for validation of theoretical approaches to model intrinsic properties of the metal-chlorates and similar species.

3.2 Experimental Methods

The general experimental approach for the IRMPD experiments using FELIX starts with ions generated using electrospray ionization (ESI) in a Micromass Z-Spray source equipped with a hexapole accumulation trap, and injected into a home-built 4.7 T FT-ICR mass spectrometer using a quadrupole deflector and an octopole guide with a potential switch that is used to slow the ions as they enter the ICR cell [21]. Instrument operating parameters, such as desolvation temperature, cone voltage, and ion accumulation and transfer optics voltages, can be optimized to increase the intensity of your ion of interest and better transfer the species to the ICR cell. Ions were accumulated for the duration of the previous FT-ICR cycle (approximately 3 s) in an external hexapole and injected into the ICR cell via a quadrupole deflector and an octapole RF ion guide. Complexes of interest were isolated before irradiation with FELIX using a stored waveform inverse Fourier transform (SWIFT) pulse [22]. Instrumentation control and data acquisition are controlled by a modular ICR data acquisition system (MIDAS) developed by the National High Field Magnetic Laboratory.

Metal chlorate solutions were generated by dissolving the appropriate salt in water to produce primary standards of 10 mM concentration, which were then further diluted with methanol to 1:5 water to methanol ratio. Instrument operating parameters, such as desolvation temperature, cone voltage, and ion accumulation and transfer optics voltages, were optimized to maximize formation of $[M(ClO_3)_2]^-$ and transfer of the species to the ICR cell. Dry nitrogen at a temperature of ~32ºC was used to assist in the desolvation process. A modified version of the

data acquisition and control hard- and software from Heeren and co-workers was used in this experiment[24]. Infrared spectra were collected by measuring the photodissociation yield as a function of photon wavelength in the range of 9-12 μm from continuously tunable IR radiation provided by the FELIX FEL[25]. Precursor $[M(ClO_3)_2]^-$ were irradiated using ten FELIX macropulses, which consists of a train of 1 ns spaced micropulses of around 1 ps duration. One macropulse has an energy of around 35 mJ, is about 5 μs long, and has a bandwidth of about 0.2 – 0.5% of the central wavelength. For the experiments discussed below, the free electron laser wavelength was tuned between 6 and 12.5 μm in 0.04 to 0.1 μm increments. The intensity of product, ClO_3^-, and undissociated precursor ions was measured using the excite/detect sequence of the FT-ICR-MS after each IRMPD step [25]. The IRMPD yield was normalized to the total ion current and linearly corrected for variations in laser power across the range scanned [23,26, 27].

3.4 Computational Methods

All electronic structure and frequency calculations were performed using the Gaussian 03 program [46] on dedicated quad-core processor workstations. Initial geometry optimization for $[Na(ClO_3)_2]^-$ and $[K(ClO_3)_2]^-$ was begun using the B3LYP functional and 6-31+G(d) basis set. The search for minima was begun using a range of precursor conformations in which the chlorates were either bidentate or tridentate ligands, or mixture of both. True minima were identified using frequency calculations at the B3LYP/6-31+G(d) level of theory. Minima located for $[Na(ClO_3)_2]^-$ and $[K(ClO_3)_2]^-$ were re-optimized using the B3LYP functional and the 6-311+G(d), 6-311+G(2d), 6-311+G(3d), 6-311+G(df), 6-311+G(2df) and 6-311+G(3df) basis sets.

To test for a general effect of basis set on predicted spectra, additional calculations were performed with the B3LYP functional and Dunning correlation-consistent double zeta (cc-pvdz) and triple zeta (cc-pvtz) basis sets, or Dunning/Huzinaga full double zeta (D95) basis sets. For the Dunning correlation consistent optimizations, five levels of theory were used: cc-pvdz, aug-cc-pvdz, aug-cc-pvdz+d, cc-pvtz and aug-cc-pvtz. For $[Na(ClO_3)_2]^-$, these basis set were applied to all atoms. The correlation consistent basis sets are not currently parameterized for K, therefore, for $[K(ClO_3)_2]^-$ these basis sets were applied to the chlorine and oxygen atoms and 6-311+G(3df) basis applied to the cation. To test further the performance of basis set on accurate modeling of Cl, calculations were also performed in which the (Dunning/Huzinaga) D95+(df), D95+(2df) and D95+(3df) basis was applied to Cl and 6-311+G(3df) basis applied to Na, K and O atoms.

As noted earlier, our overall aim was to determine the intrinsic conformation of the $[M(ClO_3)_2]^-$ species. However, an additional goal was to determine the general accuracy of the DFT calculations for prediction of vibrational frequencies for the metal-chlorate anions, as part of the development of an accurate approach for modeling these and similar species. Therefore, the frequencies generated using each functional/basis set combination, where comparisons to experimental data are made, are presented unscaled.

3.4 Results and Discussion

3.4.1 IRMPD Spectroscopy of $[M(ClO_3)_2]^-$

Representative structures for $[M(ClO_3)_2]^-$, with bidentate or tridentate coordination by chlorate, are shown in Figure 8. Bond length, bond angle and energy data for $[Na(ClO_3)_2]^-$, generated using the B3LYP functional 6-31 and 6-311 basis sets, are provided in Tables 1, 2 and

3 respectively, in the appendix. Bond length, bond angle and energy data for $[K(ClO_3)_2]^-$, using the same functional and basis sets, are provided in Tables 4, 5 and 6, respectively, also in the appendix. In Figure 8, the metal and chlorine atoms are indicated with M and Cl, respectively. Bound and unbound O atoms within the chlorate ligands are labeled with O_b and O_u, respectively.

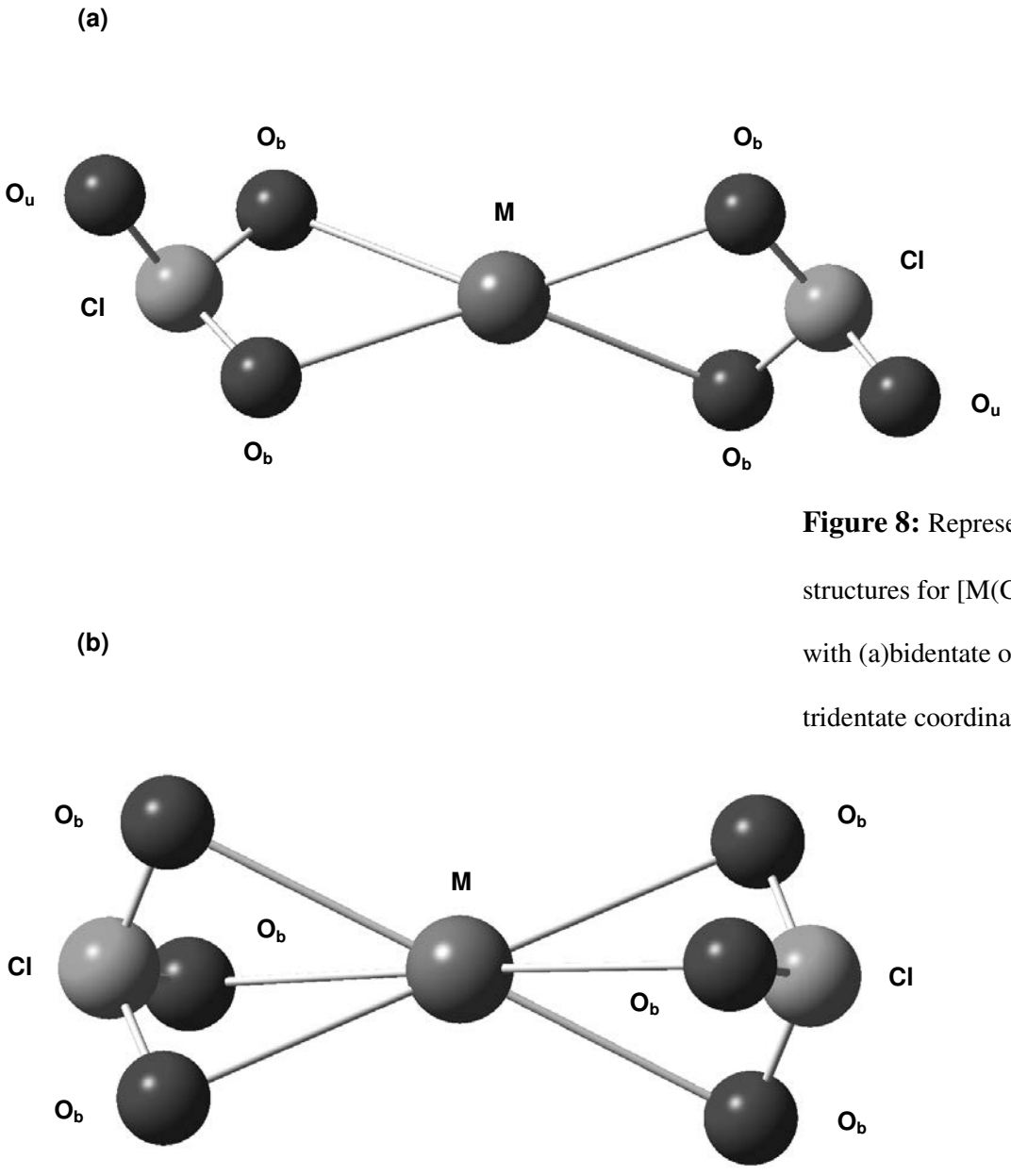

Figure 8: Representative structures for $[M(ClO_3)_2]^-$, with (a)bidentate or (b) tridentate coordination by

For both $[Na(ClO_3)_2]^-$ and $[K(ClO_3)_2]^-$, the sole photodissociation pathway observed was formation of ClO_3^- via elimination of $[M(ClO_3)]°$. Therefore, IRMPD spectra were produced for each precursor ion by monitoring the yield of ClO_3^- as a function of IR photon wavelength. The IRMPD spectrum for $[Na(ClO_3)_2]^-$, shown in Figure 9a, contains a broad feature with two distinct maxima; one centered at 939 cm^{-1} and the other at 1023 cm^{-1}.

$[M(ClO_3)_2]^-$ *Isomer*	**Frequency (cm^{-1})**	**Vibrational Mode Assignment**
M=Na		
Bidentate	916 931 1040 1046	ν_{1b} ν_{3b} ν_{3a} ν_{1a}
Tridentate	934 986	ν_1 ν_3
M=K		
Bidentate	920 938 1030 1034	ν_{1b} ν_{3b} ν_{3a} ν_{1a}
Tridentate	932 978	ν_1 ν_3

Table 12: Unscaled frequencies for theoretical *bis*-bidentate and *bis*-tridentate IR spectra at the B3LYP/6-311+G(3df) level of theory for $[Na(ClO_3)_2]^-$ and $[K(ClO_3)_2]^-$

For comparison, the spectra predicted for the *bis*-tridentate and *bis*-bidentate structures of $[Na(ClO_3)_2]^-$, at the B3LYP/6-311+G(3df) level of theory (similar patterns with respect to the number of vibrational frequencies were generated regardless of basis set choice), are shown in Figure 9b and 9c, respectively. Because of symmetry, the spectrum predicted for the *bis*-tridentate structure (figure 9b) contains a single absorption at 986 cm^{-1}, corresponding to the antisymmetric Cl-O_b stretch. The predicted spectrum for the *bis*-bidentate structure contains two absorptions that are separated by approximately 110 cm^{-1}: the splitting of the antisymmetric stretch is due to the change in binding mode of the chlorate anion. The lower frequency peak (ν_{3b}) at approximately 931 cm^{-1} corresponds to the antisymmetric O-Cl-O stretch, which involves

the O atoms coordinating the metal ion. The higher frequency stretch at 1040 cm^{-1} (ν_{3a}) corresponds instead to the terminal (unbound) Cl-O stretch. Frequency assignments are presented in Table 11.

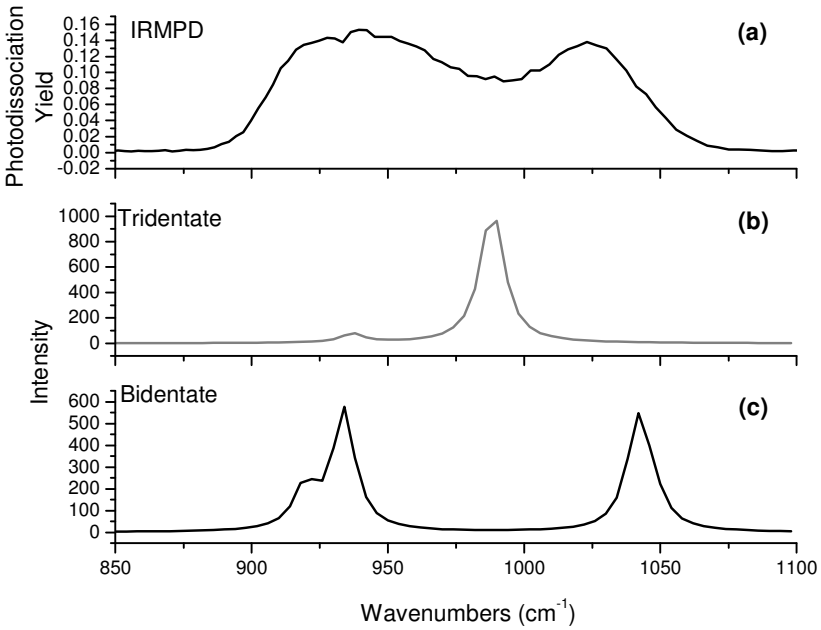

Figure 9: IR spectra for $[Na(ClO_3)_2]^-$: (a) experimental IRMPD spectrum, (b) spectrum predicted for *bis*-bidentate chlorate structure and (c) spectrum predicted for *bis*-tridentate structure. Predicted spectra were produced at the B3LYP/6-311+g(3df) level of theory.

Comparison of the experimental IRMPD spectrum and those predicted by DFT suggests that $[Na(ClO_3)_2]^-$ prefers the *bis*-bidentate structure. The two absorptions are not fully resolved in the IRMPD spectrum, which was surprising because prior studies [53] of absorptions of coordination complexes in this range were clearly resolved. The appearance of broad IRMPD resonances is not unprecedented however, especially from anionic systems that either show significant conformational flexibility such as SF_6^- [54] or have symmetrically shared hydrogen bonds such as the deprotonated amino acids aspartate and glutamate [55]. The broad nature of

the current spectra suggests that there is some degree of conformational flexibility in the complexes or a significant degree of anharmonicity in the vibrational potential surface. Therefore, the possible contribution to the IRMPD spectrum by a *bis*-tridentate structure cannot be ruled out entirely. Nonetheless, the *bis*-tridentate structure would presumably display a single prominent absorption at ca. 985 cm^{-1}, which is in the valley between the two absorptions observed in the IRMPD spectrum of $[Na(ClO_3)_2]^-$.

A strong case for the sole adoption of a *bis*-bidentate coordination structure can first be made by considering more closely the energies for the two structures derived from DFT calculations (provided for $[Na(ClO_3)_2]^-$ in Table 3 of appendix). The relative energies calculated for the *bis*-tridentate structure of $[Na(ClO_3)_2]^-$ are ~ 4 – 6 kcal/mol (~17-25 kJ/mol) higher than those predicted for the *bis*-bidentate version, depending on the basis sets employed. More importantly, for most cases the optimized tridentate conformation for $[Na(ClO_3)_2]^-$ displayed a single imaginary frequency, even with tight optimization parameters, thus establishing the structure as a saddle point rather than a true minimum.

Earlier MI-IR experiments [5], and the calculations by Solomonik and Pogrebnaya [41], suggested that two stable structures were possible for contact ion pair $[Na^+ClO_3^-]$, with chlorate bound in either a bidentate or tridentate conformation. In our later DFT investigation, at the B3LYP/6-311+G(3df) level of theory, the tridentate conformation was found to be lower in energy than the bidentate isomer by ~ 0.5 kcal/mol, consistent with the suggested presence of both isomers in the MI-IR experiments, and the low energy difference predicted by the earlier HF and MP2 calculations. The broadened peaks recorded in the IRMPD spectrum of $[Na(ClO_3)_2]^-$ may in fact be indicative of multiple structures, however the presence of the double maxima indicates that this slightly larger cluster anion, $[Na(ClO_3)_2]^-$ exists predominantly in a

bis-bidentate conformation. The unusually broad peaks could possibly be due to the "floppiness" of the chlorate ligand, allowing for slight differences in geometry within the bis-bidentate binding mode.

The IRMPD spectrum for $[K(ClO_3)_2]^-$ is shown in Figure 10a. In this case, one wide peak was observed that was centered around 960 cm^{-1} and spanning a range of 900 to 1050 cm^{-1}. The overall width of the IRMPD peak for $[K(ClO_3)_2]^-$ is nearly identical to the frequency range covered by both absorptions for the Na^+ analogue. The spectra predicted for the *bis*-tridentate and *bis*-bidentate structures of $[K(ClO_3)_2]^-$, at the B3LYP/6-311+G(3df) level of theory are provided in Figure 10b and 10c, respectively.

The theoretical spectrum predicted for the tridentate form of $[K(ClO_3)_2]^-$ is dominated by a single absorption at 978 cm^{-1} is at first glance most consistent with the broad absorption observed in the (experimental) IRMPD spectrum. However, as suggested by the data in Table 6 of the appendix, the energies of the bidentate and tridentate structures differ by only 0.1-1.4 kcal/mol (0.5-5.9 kJ/mol), and can be considered negligible when factoring in the error of the calculated energies. As for the case of the Na version of the anion, the predicted spectrum for the *bis*-bidentate structure of $[K(ClO_3)_2]^-$ contains high (ν_{3b}) and low frequency (ν_{3a}) components of ClO_3 stretch at 938 cm^{-1} and 1040 cm^{-1}, respectively.

The negligible difference in energy between the *bis*-tridentate and *bis*-bidentate forms of $[K(ClO_3)_2]^-$ opens the possibility that the IRMPD spectrum for the species reflects the presence of both isomers. Figure 10d shows a blend (50/50) of the spectra predicted for the bidentate and tridentate structures. The relative positions of the absorptions characteristic of the bidentate and

tridentate structures, when linearly combined, reproduce well the single, broad absorption measured for $[K(ClO_3)_2]^-$ by IRMPD given the resolving power of the IRMPD experiment.

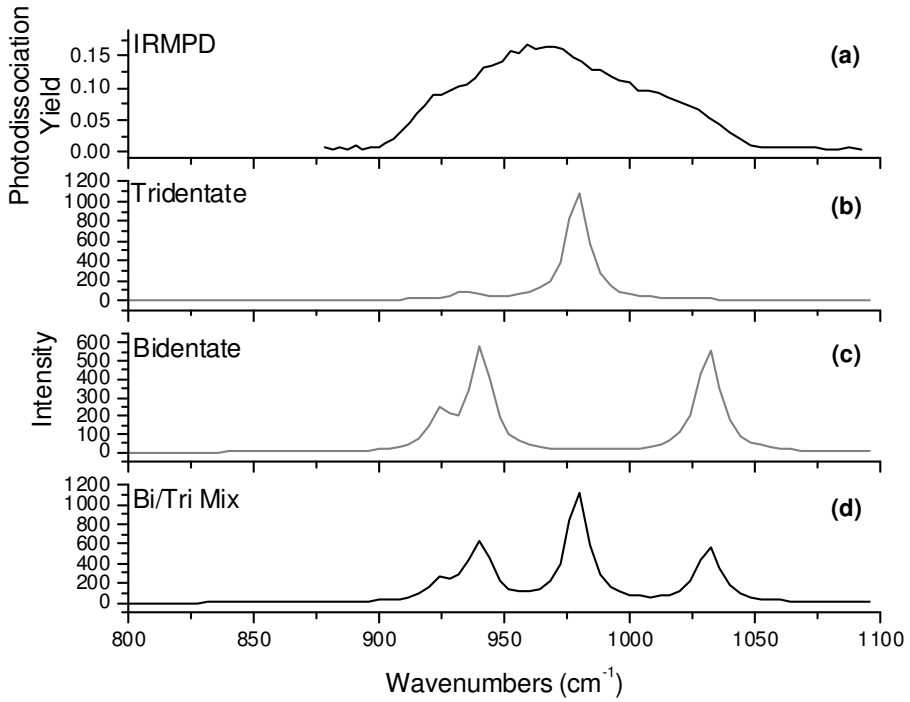

Figure 10: IR spectra for $[K(ClO_3)_2]^-$: (a) experimental IRMPD spectrum, (b) spectrum predicted for *bis*-bidentate chlorate structure, (c) spectrum predicted for *bis*-tridentate structure and (d) composite spectrum generated using a 50:50 mix of the absorptions predicted for the *bis*-bidenate and *bis*-tridentate structures. Predicted spectra were produced at the B3LYP/6-311+G(3df) level of theory.

The resolving power and/or spectral resolution for $[K(ClO_3)_2]^-$ appear to be insufficient to allow the respective absorptions to be separated. However, the agreement between the IRMPD spectrum and the blended spectrum shown in figure 10d strongly suggests that that gas-phase $[K(ClO_3)_2]^-$ likely exists as a mixture of the two isomers. This conclusion is in accord with the calculated energies for the two species. A search for stable structures which included one bidentate and one tridentate chlorate anion resulted in structures that collapsed to the *bis*-tridentate structure. When coordinates were frozen to lock the *mono*-bidentate/*mono*-tridentate

structure, a single imaginary frequency was observed in the predicted IR spectrum that corresponded to movement of the bidentate ligand towards tridentate coordination.

In our earlier DFT study of the bare metal-chlorate ion pairs, the equilibrium structure calculated for the neutral $K^+ClO_3^-$ ion pair involved only tridentate coordination by chlorate: optimizations initiated using a bidentate precursor structure resulted in collapse to the tridentate form. Using geometry constraints to force interaction between the metal cation and all three O atoms of the chlorate ligand and lock the ion pair into the bidentate structure resulted in a structure for which there was at least one imaginary frequency in the predicted infrared spectrum. However, our results in the present study clearly suggest that within the larger $[K(ClO_3)_2]^-$ anion, in the gas-phase, the ClO_3^- ligands can function as either bidentate or tridentate ligands.

The IRMPD results clearly demonstrate that the favored coordination mode (bi- versus tridentate) of chlorate depends on the metal cation. To explore this issue further, single-point energy calculations at the B3LYP/6-311+G(3df) level of theory were used to probe the complex energy as a function of metal-chlorate distance. To generate a pseudo-potential energy surface, the metal-chlorate distance was decreased by a value of 0.1 Å increments across the range of 4.5 to 2.3 Å for the *bis*-bidentate and *bis*-tridentate structures of $[Na(ClO_3)_2]^-$ and $[K(ClO_3)_2]^-$. This data for $[Na(ClO_3)_2]^-$ and $[K(ClO_3)_2]^-$ are provided in Figure 11a and 11b, respectively, in which the electronic energy difference between any point on the PES and that of the minimum is plotted as a function of the distance between the cation and the Cl atoms of the chlorate ligands.

For the *bis*-bidentate and *bis*-tridentate structures of $[Na(ClO_3)_2]^-$, the lowest energy structures were found at a distance of 3 and 2.8 Å, respectively. Within the range from 4 to ~2.7

Å, the electronic energy of the *bis*-tridentate structure is clearly higher than that for the *bis*-bidentate conformation. This observation is consistent with higher repulsion by 6 chlorate O atoms within the *bis*-tridentate structure because of the relatively small Na^+ cation. Repulsion is minimized within the *bis*-bidentate structure. For the *bis*-bidentate structure and *bis*-tridentate structure of $[K(ClO_3)_2]^-$, the lowest energy structures were found at a distance of 3.3 and 3.1 Å, respectively. More importantly, through the range of 4.5 to ~ 2.5 Å, the energy difference between the two conformations is relatively small, particularly when compared to the Na^+ analogue, consistent with the presumed adoption of both in the gas-phase by $[K(ClO_3)_2]^-$. We attribute the more possible adoption of the *bis*-tridentate conformation for K^+ to the larger ionic radius of the cation, which reduces the steric repulsion between the O atoms of the chlorate ligands.

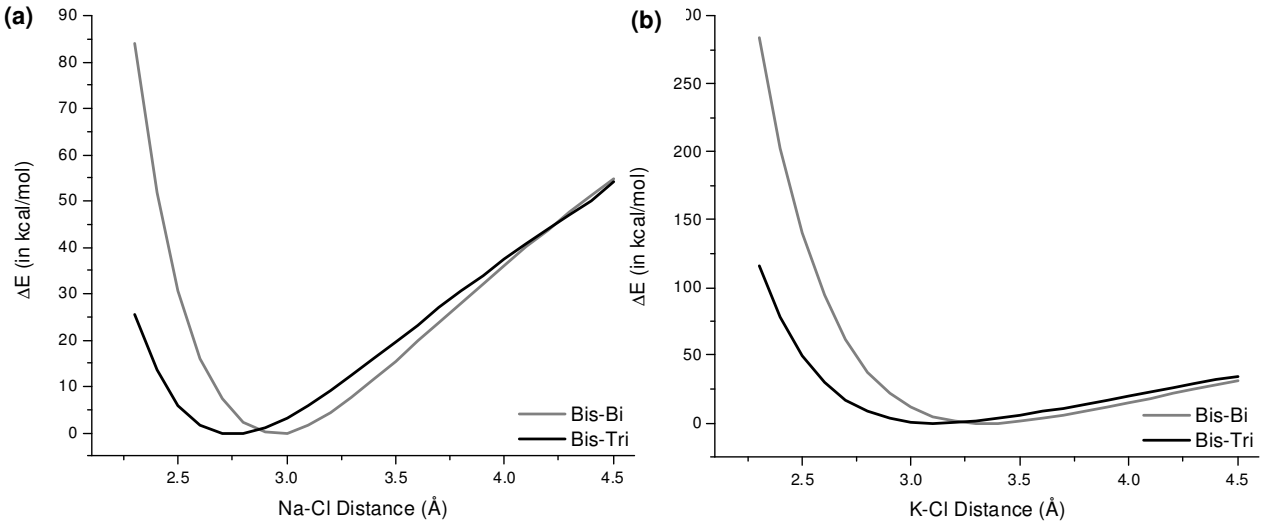

Figure 11: Comparison of ΔE to the M-Cl distance for the bis-bidentate and bis-tridentate structures of (a) $[Na(ClO_3)_2]^-$ and (b) $[K(ClO_3)_2]^-$

3.4.2 Evaluation of Computational Methods

As noted earlier, a second goal was to evaluate the accuracy of the DFT approach for determining the features of the metal-chlorate species. This goal required a somewhat systematic investigation of the qualitative and quantitative agreement between the calculated frequencies and the experimentally determined peak positions for $[Na(ClO_3)_2]^-$ and $[K(ClO_3)_2]^-$. A brief survey of the results produced by a variety of basis sets and functionals available to us is provided here.

Regardless of the functional or basis sets used, there was adequate qualitative agreement between the respective computational approaches of any one level of theory used and the experimental IRMPD spectrum. Each approach predicted 2 prominent and distinct absorptions for the *bis*-bidentate structure of $[M(ClO_3)_2]^-$ and only a single prominent absorption for the *bis*-tridentate structure. However, we found very significant quantitative differences due to choice of basis set and functional, as described below.

Comparison between the experimental IRMPD spectrum for $[Na(ClO_3)_2]^-$ and those predicted using the B3LYP functional and the 6-31+G(d), 6-311+G(d), 6-311+G(2d), 6-311+G(3d), 6-311+G(df), 6-311+G(2df) and 6-311+G(3df) basis sets are provided in Figure 1 of the appendix. Similar spectra for $[K(ClO_3)_2]^-$ are provided in Figure 2 of the appendix. When using unscaled frequencies, the best correlation between experimental and theoretical IR spectra was achieved using the 6-311+G(3df) basis set for both $[Na(ClO_3)_2]^-$ and $[K(ClO_3)_2]^-$. The smaller basis sets tend to underestimate the position of absorptions characteristic of either $[Na(ClO_3)_2]^-$ and $[K(ClO_3)_2]^-$. Use of the double zeta 6-31+G(d) basis set produces a red shift to

the respective Cl-O absorptions, when compared to spectra generated using the triple zeta 6-311+G(d), and in turn poorer quantitative agreement with the experimental IRMPD results.

Inclusion of additional diffuse d functions improves the quantitative agreement with the IRMPD values at the B3LYP/6-311 level of theory. This is shown by comparisons of frequencies generated using the 6-311+G(d) basis set with those generated with 6-311+G(3d). The same trend can be observed when f functions are included in the basis sets, for example in a comparison of frequencies generated using 6-311+G(3d) with those generated using 6-311+G(3df).

The Dunning correlation-consistent basis sets were, in general, less accurate for prediction of the chlorate stretching frequencies. The best correlation is observed at the B3LYP/cc-pvtz level of theory for $[Na(ClO_3)_2]^-$ and B3LYP/cc-pvtz/6-311+G(3df) for $[K(ClO_3)_2]^-$. Additional diffuse functions are often required for accurate modeling of anionic systems, but addition of the aug- prefix, i.e. from cc-pvdz to aug-cc-pvdz, caused a shift to lower frequencies for all absorptions, and thus surprisingly, an overall decrease in accuracy for prediction of chlorate absorptions.

Placing the Dunning/Huzinaga full double zeta (D95) basis set on the chlorine atoms resulted in agreement between experimental and theoretical frequencies that was comparable to that achieved using the 6-311 basis set, with the B3LYP/6-311+g(3df) level of theory performing slightly better for $[K(ClO_3)_2]^-$. A comparison of the IR spectra calculated for $[Na(ClO_3)_2]^-$ using B3LYP/6-311+G(3df) with the spectra calculated using B3LYP/D95+G(3df)/6-311+g(3df) showed close agreement (Figure 12). Comparison of the two basis sets approaches applied to the $[K(ClO_3)_2]^-$ complex (Figure 13) produces the same conclusion, *viz.*, very similar frequency

values are produced in each case, but the 6-311+G(3df) is shows slightly better agreement with the IRMPD data.

One case where each basis set or basis set combination produced similar results was in prediction of the degeneracy splitting of the ν_3 mode ($\Delta\nu_3$). The splitting of the mode is an important diagnostic of relative strength of metal ion binding by chlorate. As representative examples for $[Na(ClO_3)_2]^-$, average values of 109 cm^{-1} , 108 cm^{-1} and 108 cm^{-1} were predicted at the B3LYP/6-311+G(3df) , B3LYP/D95+G(3df)/6-311+G(3df) and B3LYP/cc-pvtz levels of theory, respectively, compared to 84 cm^{-1} for the IRMPD spectrum. For comparison, average values of 91 cm^{-1}, 90 cm^{-1} and 92 cm^{-1} were predicted for the splitting of $\Delta\nu_3$ for $[K(ClO_3)_2]^-$. It is difficult to assess whether the change in splitting predicted by DFT reproduces any difference in the experiment because of the broad, featureless IRMPD spectrum for $[K(ClO_3)_2]^-$. However, the predicted decrease in splitting is consistent with expected weaker interaction between ClO_3^- and K^+, relative to Na^+, and with trends predicted and observed in IRMPD studies of group II metal-nitrate anions [48, 56].

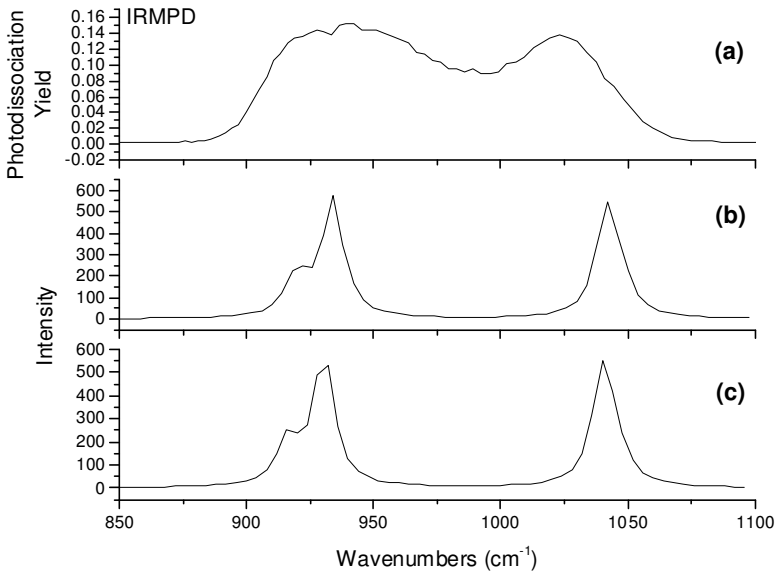

Figure 12: IR spectral comparison for $[Na(ClO_3)_2]^-$ using (a) IRMPD and theoretical calculations using the B3LYP functional and the (b) D95+G(3df)/6-311+G(3df) and (c) 6-311+G(3df) basis sets.

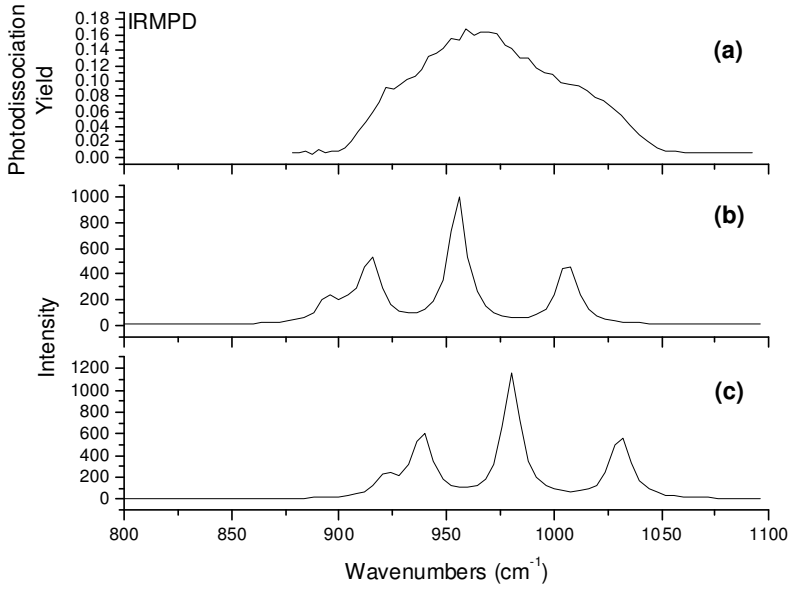

Figure 13: IR spectral comparison for $[K(ClO_3)_2]^-$ using (a) IRMPD and theoretical calculations using the B3LYP functional and the (b) D95+G(3df)/6-311+G(3df) and (c) 6-311+G(3df) basis sets.

As noted earlier, the general influence of functional and theoretical model was also evaluated. Using the 6-311+G(3df) basis set on all atoms, the best agreement between the experimental and theoretical spectra for either $[Na(ClO_3)_2]^-$ and $[K(ClO_3)_2]^-$ was achieved using the B3LYP functional. The PBEPBE functional underestimated the positioning of the chlorate absorptions, while the B3PW91, HF, LDA and MPWPW91 functionals all overestimated the positions of the same peaks. Hartree-Fock calculations, used for modeling metal-chlorate contact ion pairs in previous studies [42.43], produced the poorest correlation to the experimental IR spectra, with prediction of absorption peaks red shifted close to 200 cm^{-1} compared to the IRMPD spectra for both species. Spectra for all species are presented in the appendix.

In terms of prediction of the degeneracy splitting of the ν_3 mode ($\Delta\nu_3$), significant differences among the respective functional/models were observed. For prediction of the splitting of ν_3 for $[Na(ClO_3)_2]^-$, values of 112, 104, 112 and 104 cm^{-1} were generated using the 6-311+G(3df) basis set and PBEPBE, B3PW91, LDA and MPWPW91 functionals, respectively, compared to the experimentally measured value of 84 cm^{-1}. A predicted $\Delta\nu_3$ value of 88 cm^{-1} was obtained using HF calculations, which represents the best overall agreement with experiment. For prediction of the splitting of ν_3 for $[K(ClO_3)_2]^-$, values of 96, 88, 100 and 88 cm^{-1} were generated using PBEPBE, B3PW91, LDA and MPWPW91, respectively. A predicted $\Delta\nu_3$ value of 72 cm^{-1} was obtained using HF calculations. As with the study of effect of basis set, the decrease in splitting predicted for $[K(ClO_3)_2]^-$ is consistent with the expected decrease in strength of metal binding by chlorate.

3.5 Conclusions

In this study, the structures of gas-phase metal chlorate anions with the formula $[M(ClO_3)_2]^-$, M=Na and K, were determined using infrared multiple photon dissociation (IRMPD) spectroscopy. Experimental vibrational spectra for the two species were compared to those predicted by density functional theory for conformations featuring either bidentate or tridentate coordination of the cation by chlorate. Our results strongly suggest that the bidentate coordination mode by chlorate is preferred for $[Na(ClO_3)_2]^-$. The $[K(ClO_3)_2]^-$ instead appears to favor both bidentate and tridentate coordination. The results presented here are consistent with earlier work involving condensed-phase contact ion pairs.

The general accuracy of DFT and HF methods for predicting the positions of absorptions for both species was also evaluated. In general, the best agreement between experimental and theoretical IR spectra was achieved using the B3LYP functional and 6-311+G(3df) basis set. With the exception of PBEPBE, alternative functionals predicted IR frequencies that were shifted significantly to the blue relative to the IRMPD measurements. Use of the Dunning/Huzinaga full double zeta (D95) type basis sets on Cl, and 6-311+G(3df) and metal and oxygen, produced results comparable to the Pople triple-zeta basis sets. However, applying the Dunning correlation consistent double zeta (cc-pvdz) or triple zeta (cc-pvtz) basis sets to all atoms for which they are parameterized led to predicted frequencies that were less accurate.

REFERENCES

LIST OF REFERENCES

[1] R.S. Drago, Physical Methods of Chemists 2nd. Ed. (Surfside Scientific, Gainesville, 1992.)

[2] D. Smith, D.W. James and J.P. Devlin, J. Chem. Phys., 54 (10) (1972) 4437.

[3] G. Ritzhaupt, J.P. Devlin, J. Phys. Chem., 61 (1997) 521.

[4] G. Ritzhaupt, J.P. Devlin, J. Phys. Chem., 90 (1986) 6764.

[5] D.E. Tevault, F.K. Chi, L. Andrews, J. Mol. Spec., 51(3) (1974) 450.

[6] L. Bencivenni, K.A. Gingerich, J. Mol. Struct., 98(3-4) (1983) 195.

[7] J.P. Toth, C. Thornton and J.P. Devlin, J. Solut. Chem., 7(10) (1978) 783.

[8] N. Smyrl, J.P. Devlin, J. Phys. Chem., 77(26) (1973) 3067.

[9] G. Ritzhaupt, H.H. Richardson, J.P. Devlin, High Temp. Sci., 19(2) (1985) 163.

[10] I.R. Beattie, J.E. Parkinson, J. Chem. Soc. Dalton Trans: Inorg. Chem., 6 (1983) 1185.

[11] G. Ritzhaupt , J.P. Devlin, J. Chem. Phys., 65 (1976) 5246.

[12] L. Bencivenni, K.A. Gingerich, Inorg. Chim. Acta, 85 (1984) L11.

[13] C. Jobling, L. d'Hendercourt, A. Leger, D. Defroneau, Astron. Astrophys. 281 (1994) 923.

[14] M.A. Duncan, Int. J. Mass Spectrom. 200 (2000) 545.

[15] J.G. Black, E. Yablonovich, N. Bloembergen, S. Mukamel, Phys. Rev. Lett. 38 (1977) 1131.

[16] E.R. Grant, P.A. Schulz, A.S. Sudbo, Y.R. Shen, Y.T. Lee, Phys. Rev Lett. 40 (1978) 115.

[17] V.N. Bagratashvili, V.S. Letokov, AA Makarov, EA Ryabov. Multiple Photon Infrared Laser Photophysics and Photochemistry. (Harwood: Chur, Switzerland, 1985.)

[18] J.L. Lyman, B.E. Newman, J.W. Early, A.F.G. van der Meer. J. Phys. Chem. A. 101 (1997) 49.

[19] P.G. O'Shea, H.P. Freund, Science. 292 (2001) 1853.

[20] W.B. Colson, E.D. Johnson, M.J. Kelley, H.A. Schwettman, Phys. Today. 55 (2002) 35.

[21] N.C. Polfer NC, J. Oomens, D.T. Moore, G. von Helden, G. Meijer , R.C. Dunbar. J. Am. Chem. Soc. 128 (2006) 905.

[22] A.G. Marshall, T.C.L Wang, T.L. Ricca. J. Am. Chem. Soc. 107 (1985) 7893.

[23] A.G. Marshall, C.L. Hendrickson, G.S. Jackson. Mass Spectrom. Rev. 17 (1998) 1.

[24]] J.J. Valle, J.R. Eyler, J. Oomens, D.T. Moore, A.F.G. van der Meer, G. von Helden, G. Meijer, C.L. Hendrickson, A.G. Marshall, G.T. Blakney. Rev. Sci. Instrum. 76 (2005) 023103/1.

[25] J. Oomens J, A.G.G.M. Tielens, B.G. Sartakov, G.von Helden, G. Meijer. Astrophys. J. 591 (2003) 968.

[26] K. Burke, J.P. Perdew, Y. Wang, Electronic Density Functional Theory: Recent Progress and New Directions; Dobson, J. F.; Ed.; G. Vignale, G.; Ed.; Das, M. P.; Ed.; Plenum: New York, 1998.

[27] B. Miehlich, A. Savin, H. Stoll, H. Preuss. Chem. Phys. Lett. 157 (1989) 200.

[28] C. Lee, W. Yang, R. G. Parr, Phys. Rev. B. 37 (1988) 785.

[29] J.P. Perdew, J.A. Chevary, S.H. Vosko, K.A. Jackson, M.R. Pederson, D.J. Singh, C. Fiolhais, Phys. Rev. B. 46 (1992) 614.

[30] J.P. Perdew, J.A. Chevary, S.H. Vosko, K.A. Jackson, M.R. Pederson, D.J. Singh, C. Fiolhais, Phys. Rev. B. 48 (1993) 1024.

[31] J.P. Perdew, K. Burke, Y. Wang. Phys. Rev. B. 54 (1996) 16533.

[32] E.R. Davidson, D. Feller. Chem. Rev. 86 (1986) 681.

[33] A.D. Becke, Phys. Rev. A 38 (1988) 3098.

[34] A.D. Becke, J. Chem. Phys 98 (1993) 5648.

[35] J.C. Slater. Phys. Rev. 81 (1951) 385.

[36] S.H, Vosko, L. Wilk, M. Nusair. Can. J. Phys.58(1980) 1200.

[37] R.P. Dain, M.J. Van Stipdonk. J. Mol. Struct.: THEOCHEM. 868 (2008) 42.

[38] R.P. Dain, C.M. Leavitt, J. Oomens, J.D. Steill, G.S.Groenewold, M.J. Van Stipdonk, Rapid Comm. Mass Spectrom. 24 (2010) 232.

[39] L. Bencivenni, H.M. Nagarathna, K.A. Gingerich and R. Teghil, J. Chem. Phys., 81 (1984) 3415-23.

[40] V.G. Solomonik and T.P. Pogrebnaya, J. Struct. Chem., 39 (1998) 28-35

[41] V.G. Solomonik, T.P. Pogrebnaya and V.V. Sliznev, Zhurnal Strukturnoi Khimii., 373 (1996) 440-449.

[42] J.S. Francisco and I.H. Williams, Chem. Phys., 114 (1987) 339-345.

[43] F. Ramondo and L. Bencivenni, F. Grandinetti, Chem. Phys. Lett., 173 (1990) 562-568.

[44] M. J. Frisch, G. W. Trucks, H. B. Schlegel, G. E. Scuseria, M. A. Robb, J. R. Cheeseman, J. A. Montgomery, Jr., T. Vreven, K. N. Kudin, J. C. Burant, J. M. Millam, S. S. Iyengar, J. Tomasi, V. Barone, B. Mennucci, M. Cossi, G. Scalmani, N. Rega, G. A. Petersson, H.

Nakatsuji, M. Hada, M. Ehara, K. Toyota, R. Fukuda, J. Hasegawa, M. Ishida, T. Nakajima, Y. Honda, O. Kitao, H. Nakai, M. Klene, X. Li, J. E. Knox, H. P. Hratchian, J. B. Cross, V. Bakken, C. Adamo, J. Jaramillo, R. Gomperts, R. E. Stratmann, O. Yazyev, A. J. Austin, R. Cammi, C. Pomelli, J. W. Ochterski, P. Y. Ayala, K. Morokuma, G. A. Voth, P. Salvador, J. J. Dannenberg, V. G. Zakrzewski, S. Dapprich, A. D. Daniels, M. C. Strain, O. Farkas, D. K. Malick, A. D. Rabuck, K. Raghavachari, J. B. Foresman, J. V. Ortiz, Q. Cui, A. G. Baboul, S. Clifford, J. Cioslowski, B. B. Stefanov, G. Liu, A. Liashenko, P. Piskorz, I. Komaromi, R. L. Martin, D. J. Fox, T. Keith, M. A. Al-Laham, C. Y. Peng, A. Nanayakkara, M. Challacombe, P. M. W. Gill, B. Johnson, W. Chen, M. W. Wong, C. Gonzalez, and J. A. Pople, Gaussian 03, Revision C.02, Gaussian, Inc., Wallingford CT, 2004.

[45] G.S. Groenewold, A.K. Gianotto, K.C. Cossel, M.J. Van Stipdonk, D.T. Moore, N. Polfer, J. Oomens, W.A. de Jong and L. Visscher, J. Am. Chem. Soc., 128 (2006) 4802-4813.

[46] G.S Groenewold, A.K. Gianotto, M.E. McIlwain, M.J. Van Stipdonk, M. Kullman, D.T. Moore, N. Polfer and J. Oomens, J. Phys. Chem. A., 112 (2008) 508-521.

[47] G.S. Groenewold, J. Oomens, W.A. de Jong, G.L. Gresham, M.E. McIlwain and M.J. Van Stipdonk, Phys. Chem.-Chem. Phys., 10 (2008) 1192-1202.

[48] J. Oomens, L. Myers, R.P. Dain, C.M. Leavitt, V. Pham, G. Gresham, G. Groenewold and M.J. Van Stipdonk, Int. J. Mass Spectrom. 2008, 273 (2008) 24-30.

[49] D. Oepts, A.F.G. van der Meer, P.W. van Amersfoort. Infrared Phys. Technol. 36 (1995) 297.

[50] A.G. Marshall, T.C.L. Wang, T.L. Ricca. J. Am. Chem. Soc. 107 (1985) 7893.

[51] T.H Mize, I. Taban, M. Duursma, M. Seynen, M. Konijnenburg, A. Vijftigschild, C.V. Doornik, G.V. Rooij, R.M.A. Heeren. Int. J. Mass Spectrom. 235 (2004) 243.

[52] D.T. Moore, J. Oomens, J.R. Eyler, G. von Helden, G. Meijer, R.C. Dunbar. J. Am. Chem. Soc. 127 (2005) 7243.

[53] G.S. Groenewold, J. Oomens, W.A. de Jong, G.L. Gresham, M.E. McIlwain, M.J. Van Stipdonk. Phys. Chem-Chem. Phys. 10 (2008) 1192.

[54] J.D. Steill, J. Oomens, J.R. Eyler, R.N. Compton. J. Chem. Phys. 129 (2008) 244302.

[55] J. Oomens, J.D. Steill, B. Redlich, J. Amer. Chem Soc. 131 (2009) 4310.

[56] C.M. Leavitt, J. Oomens, R.P. Dain, J.D. Steill, G.S. Groenewold, M.J. Van Stipdonk. J. Am. Soc. Mass Spectrom. 20 (2009) 722.

APPENDIX

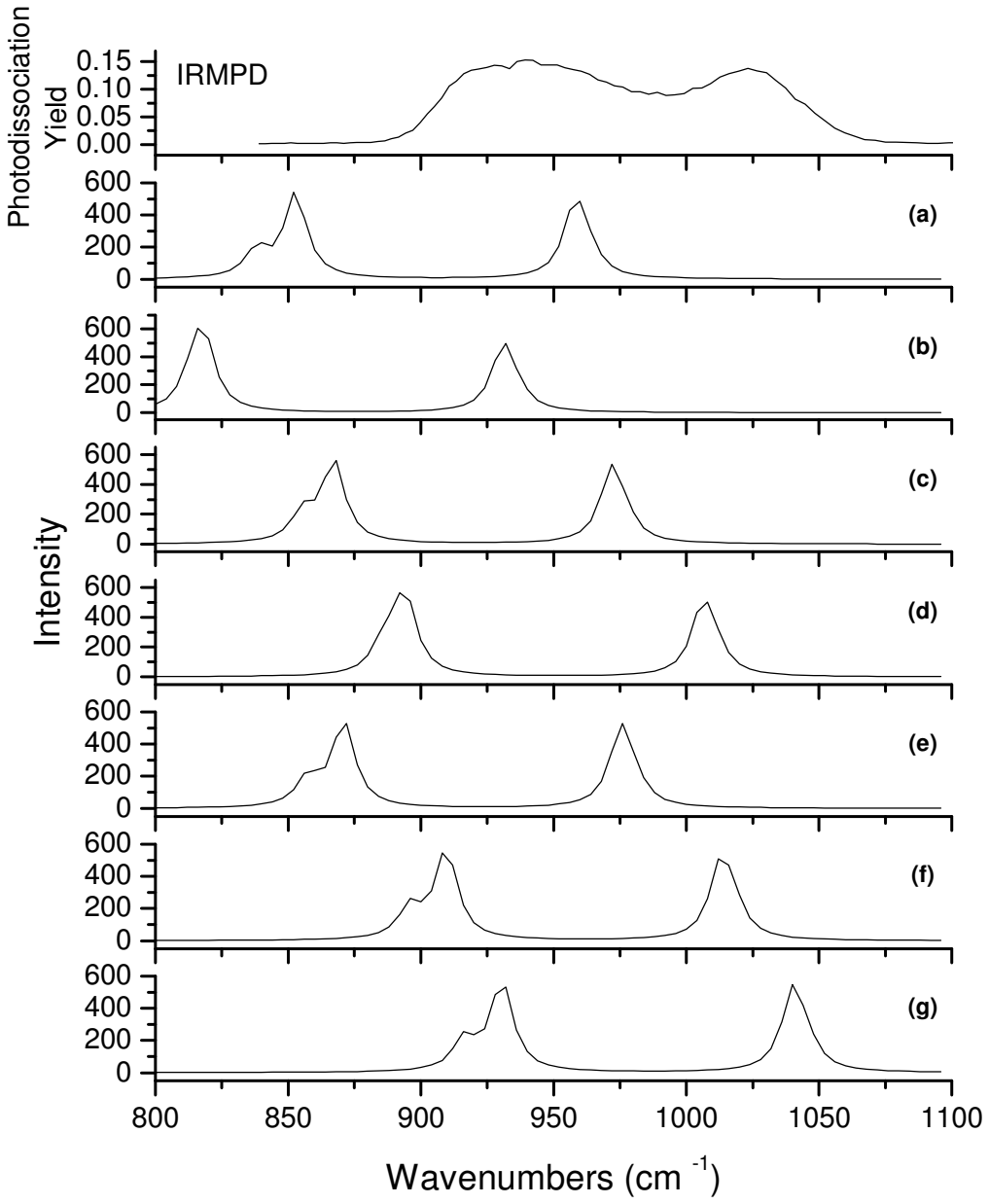

Figure A-1: Experimental and theoretical IR spectral comparison for $[Na(ClO_3)_2]^-$ using the B3LYP functional and the (a) 6-31+G(d), (b) 6-311+G(d), (c) 6-311+G(2d), (d) 6-311+G(3d), (e) 6-311+G(df), (f) 6-311+G(2df) and (g) 6-311+G(3df) basis sets.

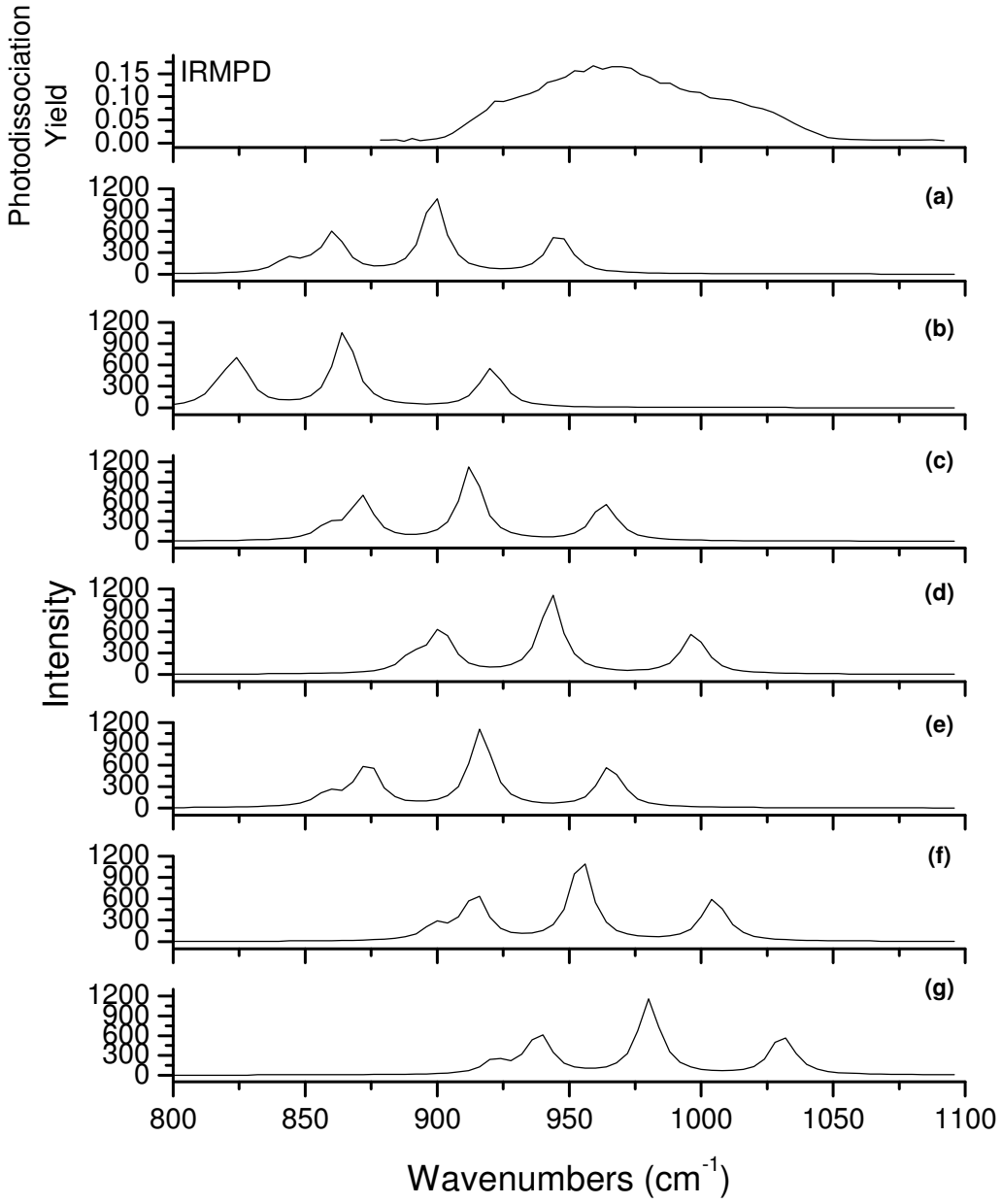

Figure A-2: Experimental and theoretical IR spectral comparison for a 1:1 mixture of bis-bi- and bis-tri-dentate complexes of $[K(ClO_3)_2]^-$ using the B3LYP functional and the (a) 6-31+G(d), (b) 6-311+G(d), (c) 6-311+G(2d), (d) 6-311+G(3d), (e) 6-311+G(df), (f) 6-311+G(2df) and (g) 6-311+G(3df) basis sets.

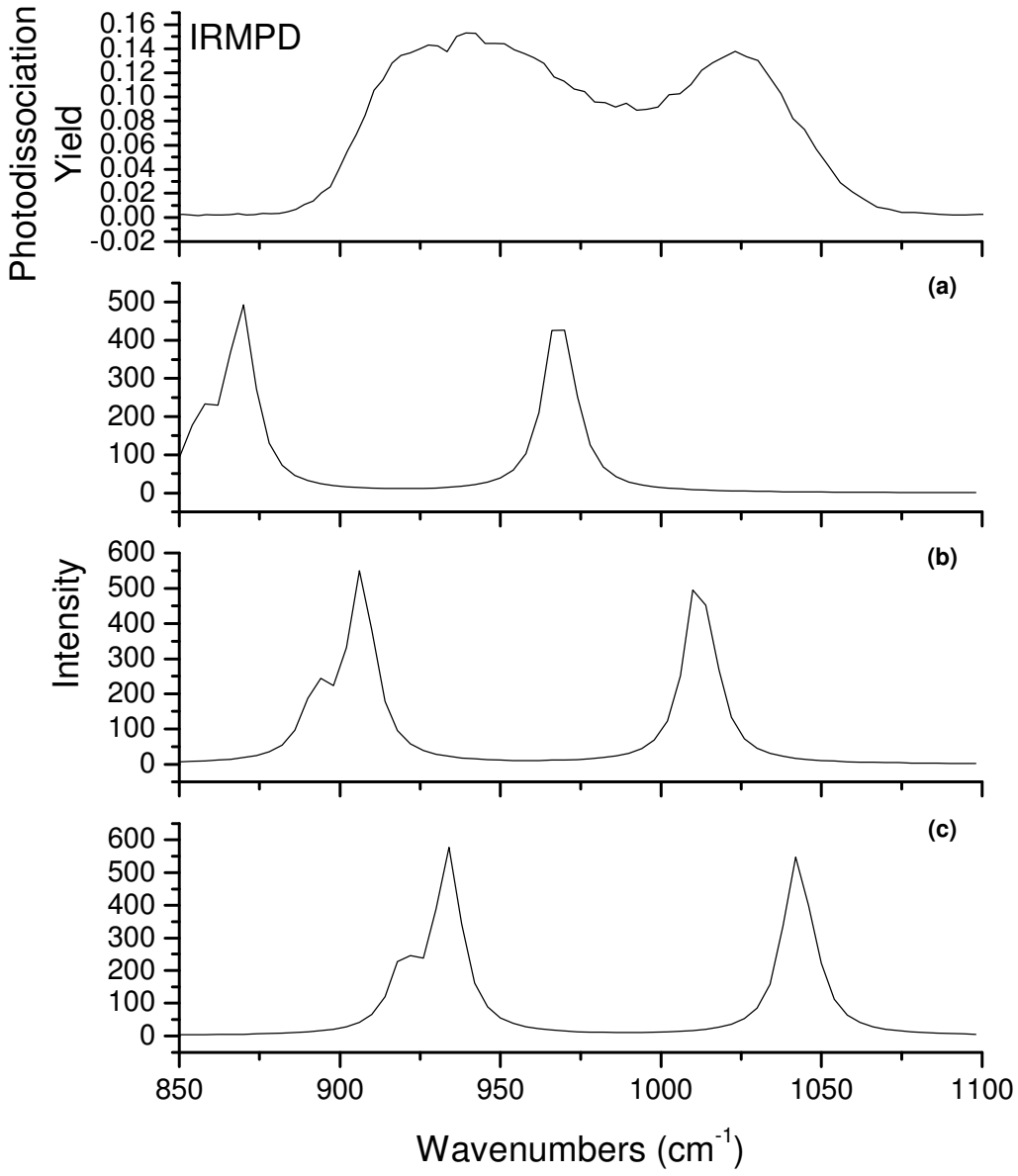

Figure A-3: Experimental and theoretical IR spectral comparison for $[Na(ClO_3)_2]^-$ using the B3LYP functional and the (a) D95+G(df)/6-311+G(3df), (b) D95+G(2df)/6-311+G(3df) and (c) D95+G(3df)/6-311+G(3df) basis set combinations

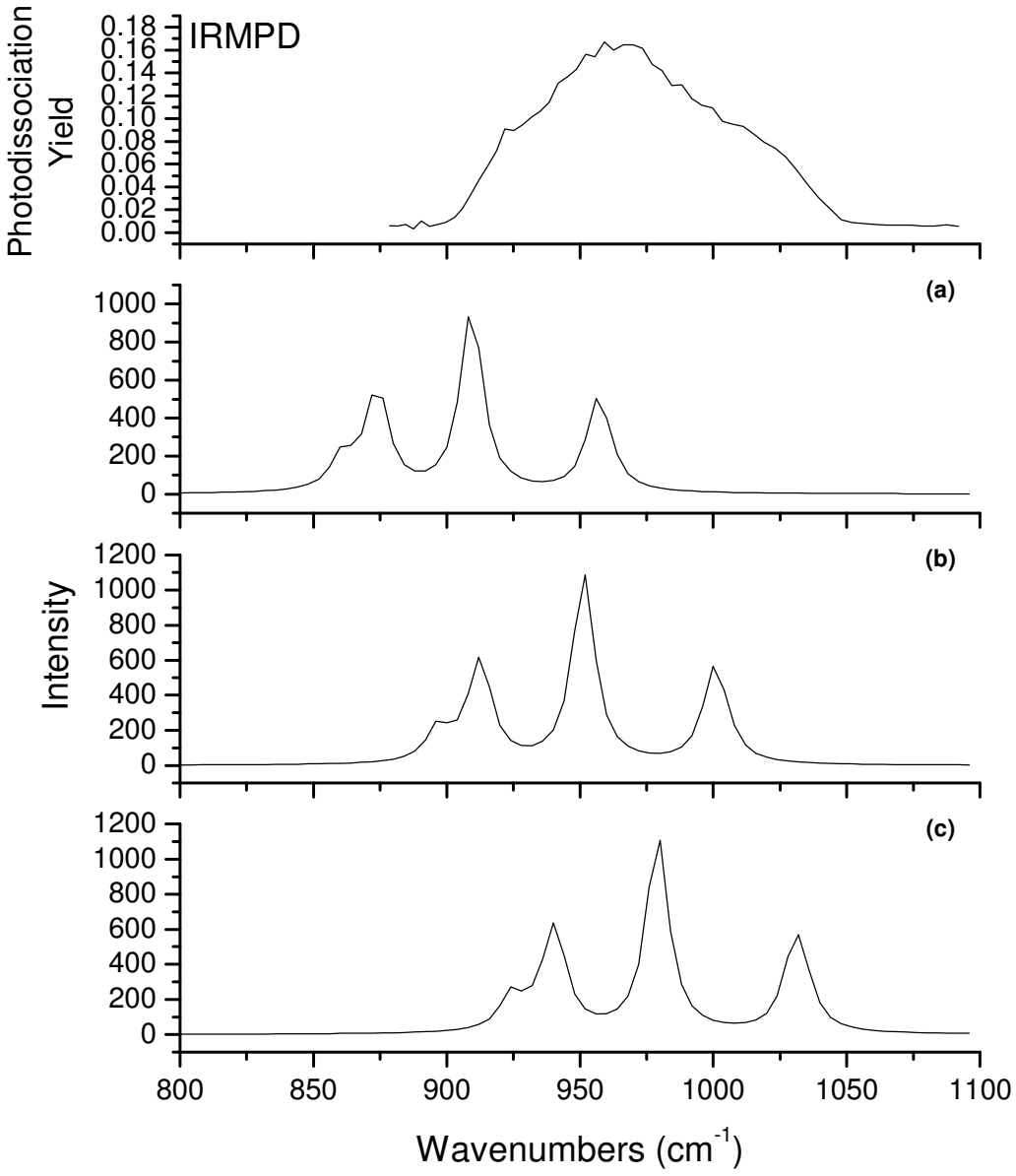

Figure A-4: Experimental and theoretical IR spectral comparison for a 1:1 mixture of bis-bi- and bis-tri-dentate complexes of $[K(ClO_3)_2]^-$ using the B3LYP functional and the (a) D95+G(df)/6-311+G(3df), (b) D95+G(2df)/6-311+G(3df) and (c) D95+G(3df)/6-311+G(3df) basis set combinations

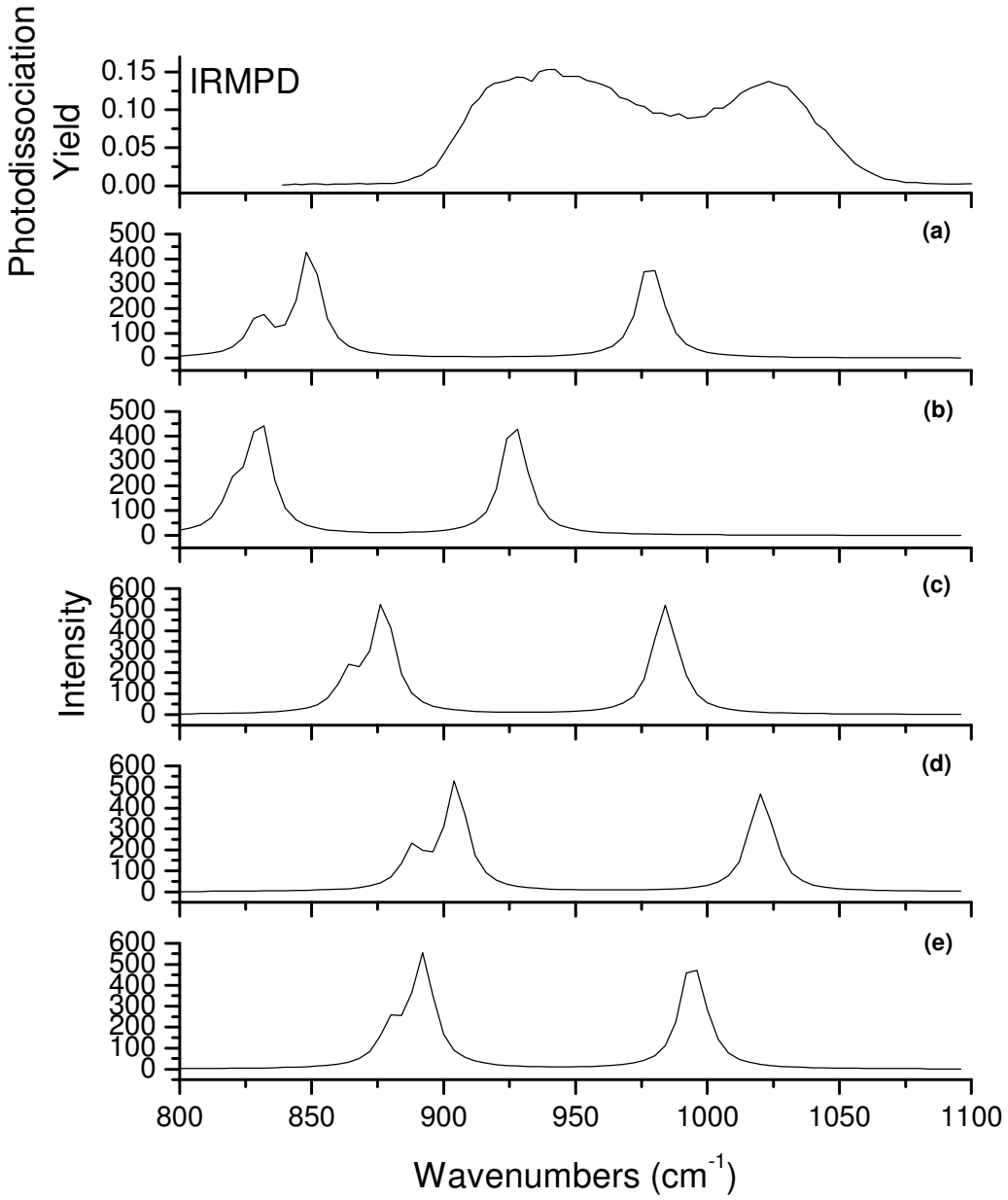

Figure A-5: Experimental and theoretical IR spectral comparison for $[Na(ClO_3)_2]^-$ using the B3LYP functional and the (a) cc-pvdz, (b) aug- cc-pvdz, (c) aug- cc-pvdz+d, (d) cc-pvtz and (e) aug-cc-pvtz basis set.

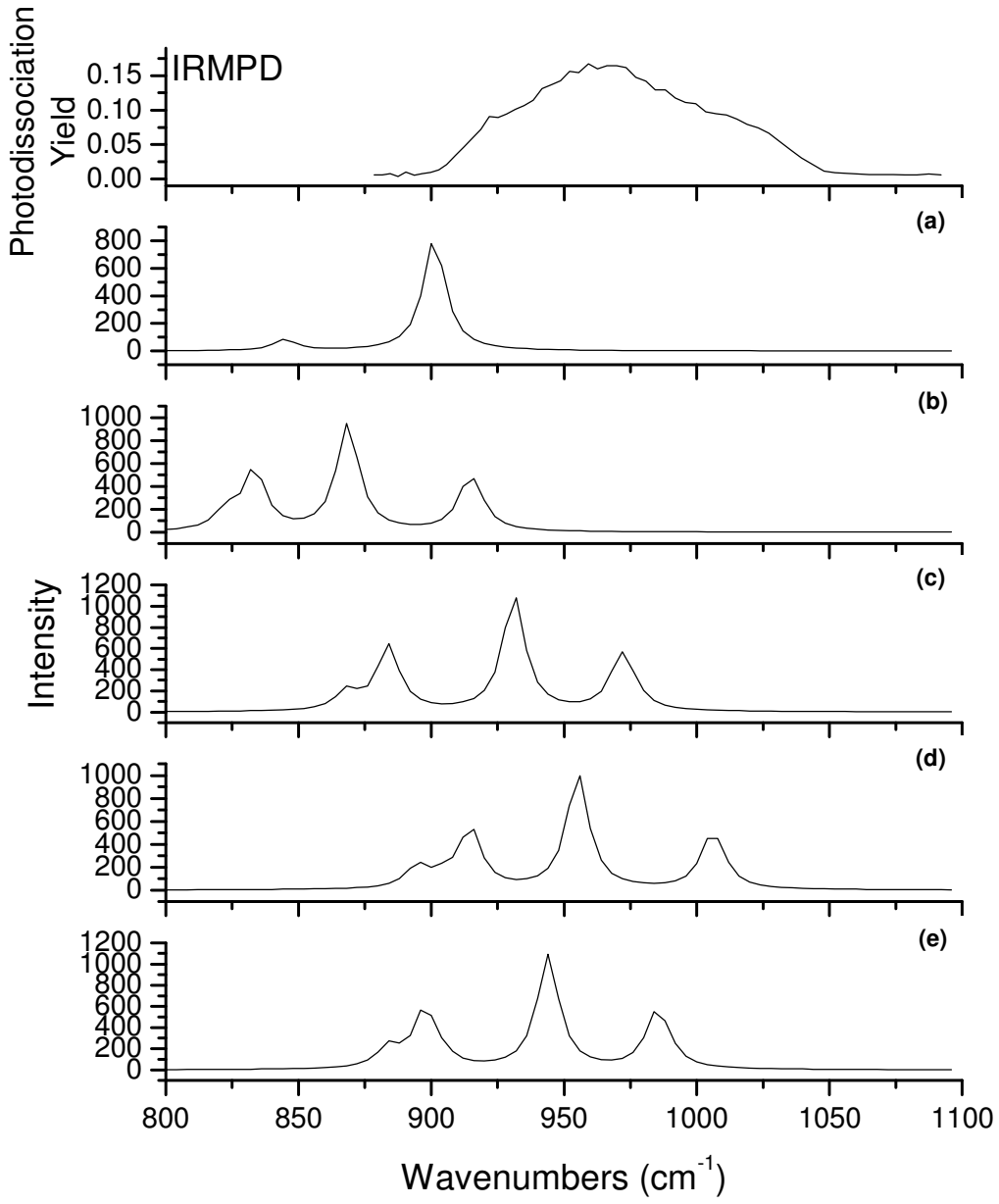

Figure A-6: Experimental and theoretical IR spectral comparison for a 1:1 mixture of bis-bi- and bis-tri-dentate complexes of $[K(ClO_3)_2]^-$ using the B3LYP functional and the (a) cc-pvdz/6-311+G(3df), (b) aug- cc-pvdz/6-311+G(3df), (c) aug- cc-pvdz+d/6-311+G(3df), (d) cc-pvtz/6-311+G(3df) and (e) aug-cc-pvtz/6-311+G(3df) basis set combinations.

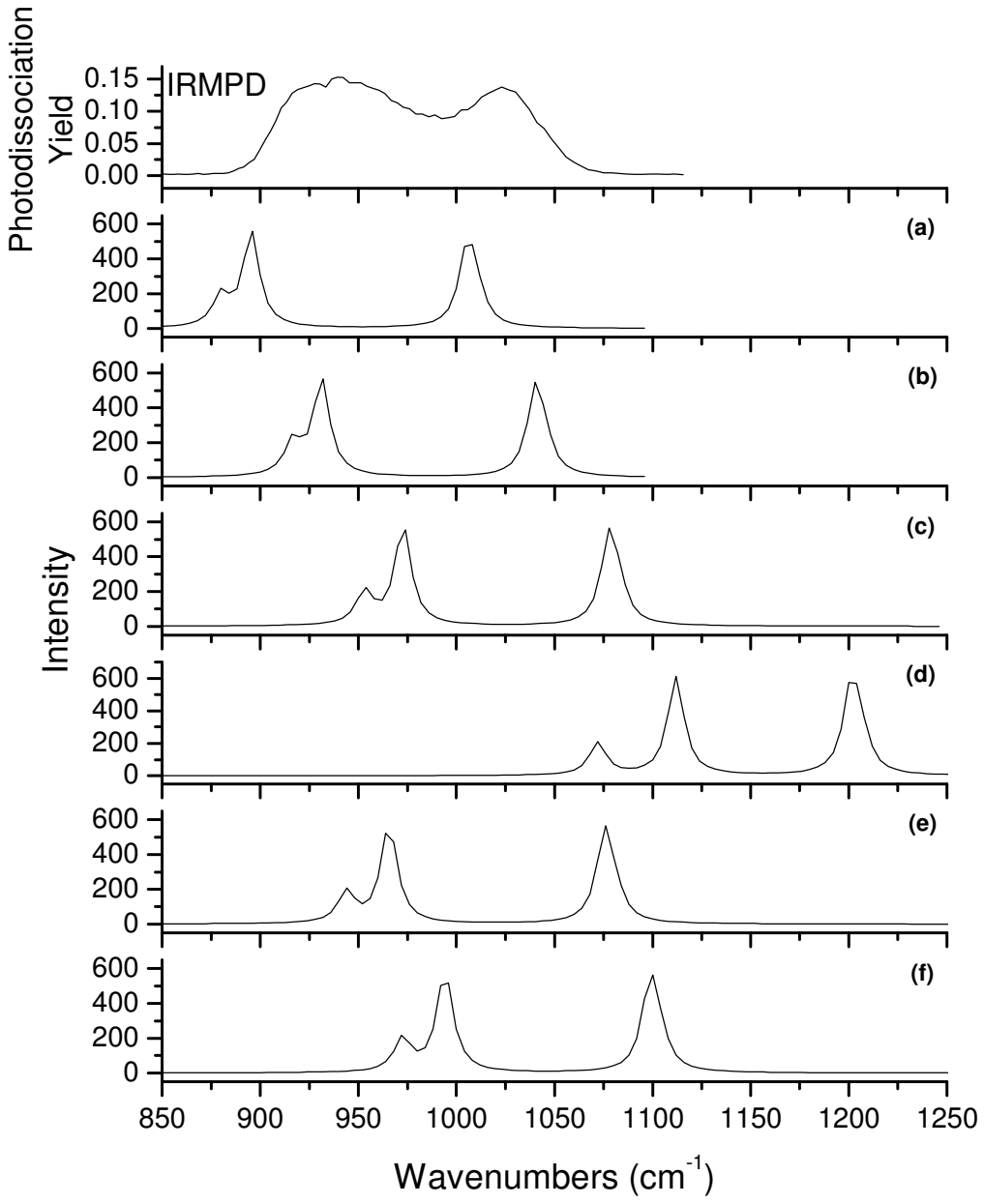

Figure A-7: Experimental and theoretical IR spectral comparison for $[Na(ClO_3)_2]^-$ using the 6-311+G(3df) basis set and the (a) PBEPBE functional , (b) B3LYP functional, (c) B3PW91 functional, (d) HF model, (e) LDA functional and (f) MPWPW91 functional.

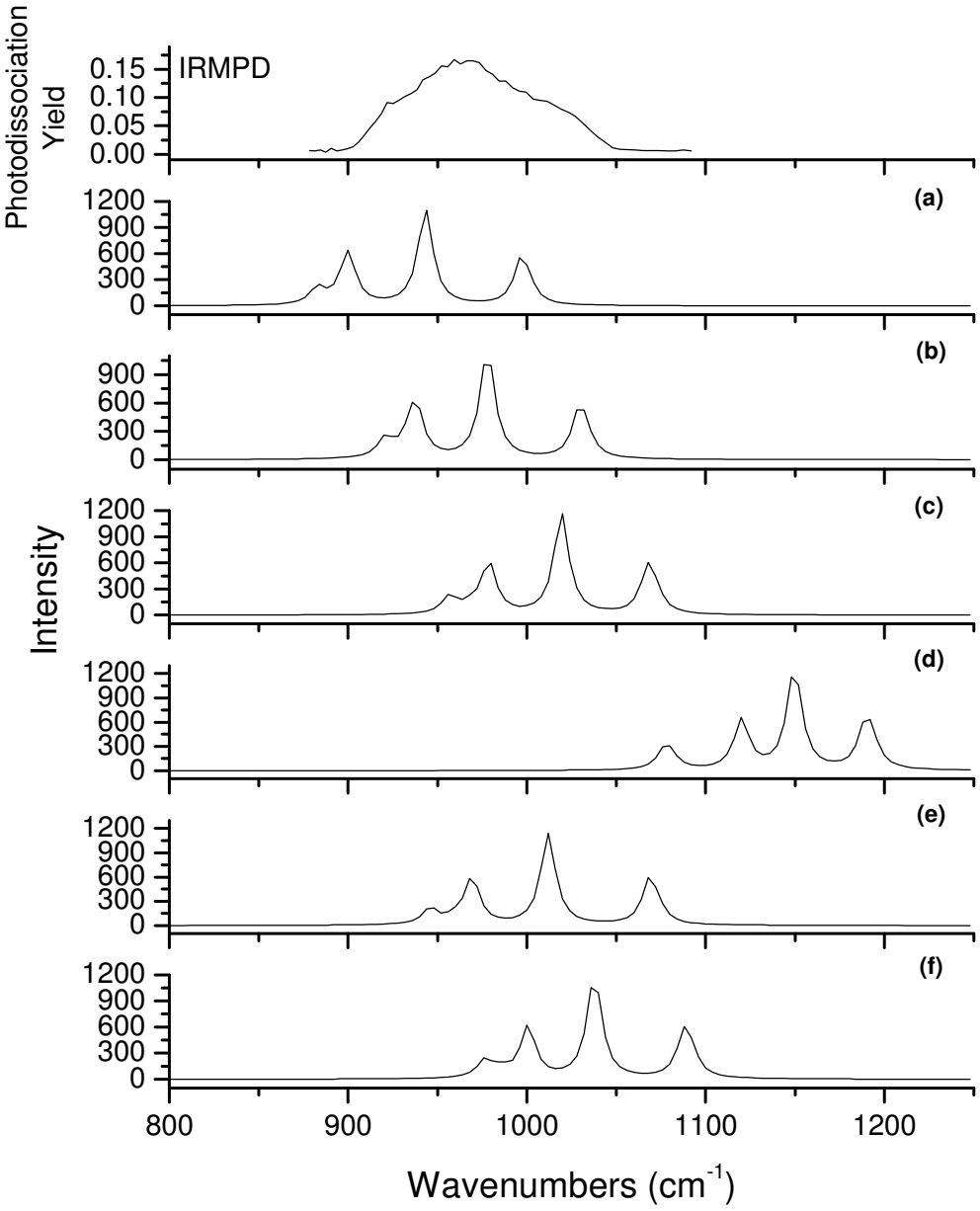

Figure A-8: Experimental and theoretical IR spectral comparison for a 1:1 mixture of bis-bi- and bis-tri-dentate complexes of $[K(ClO_3)_2]^-$ using the 6-311+G(3df) basis set and the (a) PBEPBE functional , (b) B3LYP functional, (c) B3PW91 functional, (d) HF model, (e) LDA functional and (f) MPWPW91 functional.

Basis Set *Conformation*	**Cl-O_u**	**Cl-O_b**	**M-O**	**M-Cl**
B3LYP/6-31+G(d)				
Bidentate	1.520	1.558	2.335	2.943
Tridentate	-	1.543	2.598	2.767
B3LYP/6-311+G(d)				
Bidentate	1.515	1.558	2.350	2.964
Tridentate	-	1.541	2.606	2.779
B3LYP/6-311+G(2d)				
Bidentate	1.496	1.536	2.350	2.964
Tridentate	-	1.520	2.593	2.764
B3LYP/6-311+G(3d)				
Bidentate	1.482	1.520	2.340	2.951
Tridentate	-	1.506	2.574	2.764
B3LYP/6-311+G(df)				
Bidentate	1.504	1.542	2.331	2.936
Tridentate	-	1.528	2.574	2.746
B3LYP/6-311+G(2df)				
Bidentate	1.485	1.522	2.348	2.947
Tridentate	-	1.508	2.587	2.746
B3LYP/6-311+G(3df)				
Bidentate	1.473	1.509	2.342	2.937
Tridentate	-	1.496	2.577	2.750

Table A-1: Bond Lengths (in Å) for $[Na(ClO_3)_2]^-$ isomers using the B3LYP functional and Pople basis sets.

Basis Set *Conformation*	**O_b-Cl-O_b**	**O_u-Cl-O_b**	**Cl-O_b-M**	**O_u-Cl-M**
B3LYP/6-31+G(d)				
Bidentate	104.182	109.296	96.100	121.608
Tridentate	106.116	-	79.413	-
B3LYP/6-311+G(d)				
Bidentate	103.837	109.473	96.617	122.748
Tridentate	106.063	-	79.796	-

B3LYP/6-311+G(2d)				
Bidentate	104.461	108.879	96.603	119.474
Tridentate	106.063	-	79.837	-
B3LYP/6-311+G(3d)				
Bidentate	104.574	108.794	96.758	120.101
Tridentate	106.167	-	79.923	-
B3LYP/6-311+G(df)				
Bidentate	104.118	109.095	96.479	121.325
Tridentate	105.984	-	79.594	-
B3LYP/6-311+G(2df)				
Bidentate	104.488	108.629	96.871	119.083
Tridentate	106.124	-	88.105	-
B3LYP/6-311+G(3df)				
Bidentate	104.599	108.629	96.997	119.819
Tridentate	106.167	-	88.182	-

Table A-2: Bond Angles (in °) for $[Na(ClO_3)_2]^-$ isomers using the B3LYP functional and Pople basis sets

Basis Set *Conformation*	**Uncorr.**	**ZPEC**	**ZPE**	**ΔE (kcal/mol)**
B3LYP/6-31+G(d)				
Bidentate	-1533.7358	0.0209	-1533.7148	0
Tridentate	-1533.7253	0.0197	-1533.7056	+5.7731
B3LYP/6-311+G(d)				
Bidentate	-1533.9070	0.0205	.-1533.8866	0
Tridentate	-1533.8961	0.0193	-1533.8768	+6.1496
B3LYP/6-311+G(2d)				
Bidentate	-1533.9924	0.0205	-1533.9711	0
Tridentate	-1533.9845	0.0203	-1533.9642	+4.3298
B3LYP/6-311+G(3d)				
Bidentate	-1534.0238	0.0220	-1534.0016	0
Tridentate	-1534.0162	0.0211	-1533.9950	+4.1416
B3LYP/6-311+G(df)				
Bidentate	-1533.9605	0.0214	-1533.9390	0
Tridentate	-1533.9496	0.0201	-1533.9295	+5.9613

B3LYP/6-311+G(2df)				
Bidentate	-1534.0404	0.0222	-1534.0183	0
Tridentate	-1534.0327	0.0211	-1534.0116	+4.2043
B3LYP/6-311+G(3df)				
Bidentate	-1534.0674	0.0227	.-1534.0447	0
Tridentate	-1534.0599	0.0217	-1534.0381	+4.1416

Table A-3: Energies for $[Na(ClO_3)_2]^-$ isomers using the B3LYP functional and Pople basis sets.

Basis Set *Conformation*	**Cl-O_u**	**Cl-O_b**	**M-O**	**M-Cl**
B3LYP/6-31+G(d)				
Bidentate	1.524	1.555	2.744	3.381
Tridentate	-	1.545	2.942	3.149
B3LYP/6-311+G(d)				
Bidentate	1.543	1.555	2.718	3.367
Tridentate	-	1.543	2.936	3.145
B3LYP/6-311+G(2d)				
Bidentate	1.499	1.534	2.718	3.338
Tridentate	-	1.522	2.915	3.123
B3LYP/6-311+G(3d)				
Bidentate	1.485	1.518	2.698	3.324
Tridentate	-	1.507	2.906	3.114
B3LYP/6-311+G(df)				
Bidentate	1.507	1.540	2.719	3.365
Tridentate	-	1.528	2.928	3.139
B3LYP/6-311+G(2df)				
Bidentate	1.489	1.520	2.709	3.339
Tridentate	-	1.510	2.915	3.127
B3LYP/6-311+G(3df)				
Bidentate	1.476	1.507	2.701	3.326
Tridentate	-	1.497	2.905	3.115

Table A-4: Bond Lengths (in Å) for $[K(ClO_3)_2]^-$ isomers using the B3LYP functional and Pople basis sets.

Basis Set *Conformation*	**O_b-Cl-O_b**	**O_u-Cl-O_b**	**Cl-O_b-M**	**O_u-Cl-M**
B3LYP/6-31+G(d)				
Bidentate	105.476	108.825	100.011	115.295
Tridentate	106.821	-	82.884	-
B3LYP/6-311+G(d)				
Bidentate	105.025	109.056	100.426	119.812
Tridentate	106.723	-	82.955	-
B3LYP/6-311+G(2d)				
Bidentate	105.702	108.482	100.114	116.488
Tridentate	106.776	-	83.110	-
B3LYP/6-311+G(3d)				
Bidentate	105.819	108.430	100.319	118.098
Tridentate	106.784	-	83.321	-
B3LYP/6-311+G(df)				
Bidentate	104.998	108.293	100.730	119.311
Tridentate	106.651	-	83.256	-
B3LYP/6-311+G(2df)				
Bidentate	105.604	108.293	100.463	116.668
Tridentate	106.784	-	83.468	-
B3LYP/6-311+g(3df)				
Bidentate	105.724	108.315	100.621	117.905
Tridentate	106.728	-	83.584	-

Table A-5: Bond Angles (in °) for $[K(ClO_3)_2]^-$ isomers using the B3LYP functional and Pople basis sets.

Basis Set *Conformation*	**Uncorr.**	**ZPEC**	**ZPE**	**ΔE (kcal/mol)**
B3LYP/6-31+G(d)				
Bidentate	-1971.3397	0.0202	-1971.3195	0
Tridentate	-1971.3392	0.0199	-1971.3193	+0.1255
B3LYP/6-311+G(d)				
Bidentate	-1971.5432	0.0197	-1971.5235	0
Tridentate	-1971.5406	0.0193	-1971.5213	+1.3805
B3LYP/6-311+g(2d)				

Bidentate	-1971.6283	0.0206	-1971.6076	0
Tridentate	-1971.6279	0.0204	-1971.6074	+0.1255
B3LYP/6-311+G(3d)				
Bidentate	-1971.6594	0.0214	-1971.6380	0
Tridentate	-1971.6590	0.0211	-1971.6379	+0.0628
B3LYP/6-311+G(df)				
Bidentate	-1971.5927	0.0205	-1971.5722	0
Tridentate	-1971.5906	0.0201	-1971.5704	+1.1295
B3LYP/6-311+G(2df)				
Bidentate	-1971.6758	0.0215	-1971.6543	0
Tridentate	-1971.6754	0.0212	-1971.6541	+0.1255
B3LYP/6-311+G(3df)				
Bidentate	-1971.7029	0.0221	-1971.6808	0
Tridentate	-1971.7023	0.0217	-1971.6806	+0.1255

Table A-6: Energies for $[K(ClO_3)_2]^-$ isomers using the B3LYP functional and Pople basis sets

Basis Set *Conformation*	**Cl-O_u**	**Cl-O_b**	**M-O**	**M-Cl**
B3LYP/D95+(df)/6-311+G(3df)				
Bidentate	1.517	1.555	2.346	2.953
Tridentate	-	1.514	2.592	2.771
B3LYP/D95+(2df)/6-311+G(3df)				
Bidentate	1.489	1.525	2.343	2.942
Tridentate	-	1.512	2.581	2.757
B3LYP/D95+(3df)/6-311+G(3df)				
Bidentate	1.476	1.512	2.342	2.938
Tridentate	-	1.499	2.581	2.756

Table A-7: Bond Lengths (in Å) for $[Na(ClO_3)_2]^-$ isomers using the B3LYP functional and Dunning/Huzinaga full double zeta basis sets

Basis Set *Conformation*	**O_b-Cl-O_b**	**O_u-Cl-O_b**	**Cl-O_b-M**	**O_u-Cl-M**
B3LYP/D95+(df)/6-311+G(3df)				
Bidentate	104.275	108.592	96.291	119.683
Tridentate	106.234	-	78.632	-
B3LYP/D95+(2df)/6-311+G(3df)				
Bidentate	104.480	108.545	96.748	119.231
Tridentate	106.000	-	80.063	-
B3LYP/D95+(3df)/6-311+G(3df)				
Bidentate	104.594	108.621	96.949	119.653
Tridentate	106.142	-	80.210	-

Table A-8: Bond Angles (in °) for $[Na(ClO_3)_2]^-$ isomers using the B3LYP functional and Dunning/Huzinaga full double zeta basis sets

Basis Set *Conformation*	**Uncorr.**	**ZPEC**	**ZPE**	**ΔE (kcal/mol)**
B3LYP/D95+(df)/6-311+G(3df)				
Bidentate	-1533.9164	0.0197	-1533.8952	0
Tridentate	-1533.9081	0.0202	-1533.8879	+4.5808
B3LYP/D95+(2df)/6-311+G(3df)				
Bidentate	-1533.9685	0.0221	-1533.9463	0
Tridentate	-1533.9607	0.0211	-1533.9396	+4.2043
B3LYP/D95+(3df)/6-311+G(3df)				
Bidentate	-1534.0022	0.0227	-1533.9795	0
Tridentate	-1533.9943	0.0217	-1533.9726	+4.3298

Table A-9: Energies for $[Na(ClO_3)_2]^-$ isomers using the B3LYP functional and Dunning/Huzinaga full double zeta basis sets

Basis Set *Conformation*	**Cl-O_u**	**Cl-O_b**	**M-O**	**M-Cl**
B3LYP/D95+(df)/6-311+G(3df)				

Bidentate	1.521	1.552	2.707	3.344
Tridentate	-	1.542	2.909	3.120
B3LYP/D95+(2df)/6-311+G(3df)				
Bidentate	1.492	1.523	2.703	3.332
Tridentate	-	1.513	2.902	3.124
B3LYP/D95+(3df)/6-311+G(3df)				
Bidentate	1.480	1.510	2.702	3.328
Tridentate	-	1.500	2.907	3.117

Table A-10: Bond Lengths (in Å) for $[K(ClO_3)_2]^-$ isomers using the B3LYP functional and Dunning/Huzinaga full double zeta basis sets

Basis Set *Conformation*	**O_b-Cl-O_b**	**O_u-Cl-O_b**	**Cl-O_b-M**	**O_u-Cl-M**
B3LYP/D95+(df)/6-311+G(3df)				
Bidentate	105.523	108.221	99.920	116.905
Tridentate	106.490	-	82.940	-
B3LYP/D95+(2df)/6-311+G(3df)				
Bidentate	105.642	108.208	100.357	117.071
Tridentate	106.600	-	83.354	-
B3LYP/D95+(3df)/6-311+G(3df)				
Bidentate	105.732	108.289	100.551	117.614
Tridentate	106.729	-	83.507	-

Table A-11: Bond Angles (in °) for $[K(ClO_3)_2]^-$ isomers using the B3LYP functional and Dunning/Huzinaga full double zeta basis sets

Basis Set *Conformation*	**Uncorr.**	**ZPEC**	**ZPE**	**ΔE (kcal/mol)**
B3LYP/D95+(df)/6-311+G(3df)				
Bidentate	-1971.5513	0.0205	-1971.5308	+0.1883
Tridentate	-1971.5513	0.0202	-1971.5311	0
B3LYP/D95+(2df)/6-311+G(3df)				

Bidentate	-1971.6036	0.0214	-1971.5822	+0.1255
Tridentate	-1971.5824	0.0212	-1971.5824	0
B3LYP/D95+(3df)/6-311+G(3df)				
Bidentate	-1971.6376	0.0220	-1971.6156	0
Tridentate	-1971.6372	0.0217	-1971.6155	+0.0627

Table A-12: Energies for $[K(ClO_3)_2]^-$ isomers using the B3LYP functional and Dunning/Huzinaga full double zeta basis sets

Basis Set *Conformation*	**Cl-O_u**	**Cl-O_b**	**M-O**	**M-Cl**
B3LYP/cc-pvdz				
Bidentate	1.525	1.572	2.312	2.907
Tridentate	-	1.555	2.574	2.732
B3LYP/aug-cc-pvdz				
Bidentate	1.537	1.576	2.348	2.958
Tridentate	Collapsed To Bidentate			
B3LYP/aug-cc-pvdz+d				
Bidentate	1.502	1.540	2.340	2.940
Tridentate	-	1.526	2.595	2.764
B3LYP/cc-pvtz				
Bidentate	1.491	1.529	2.344	2.936
Tridentate	-	1.515	2.580	2.750
B3LYP/aug- cc-pvtz				
Bidentate	1.495	1.531	2.351	2.951
Tridentate	-	1.518	2.588	2.763

Table A-13: Bond Lengths (in Å) for $[Na(ClO_3)_2]^-$ isomers using the B3LYP functional and Dunning correlation consistent basis sets

Basis Set *Conformation*	**O_b-Cl-O_b**	**O_u-Cl-O_b**	**Cl-O_b-M**	**O_u-Cl-M**
B3LYP/cc-pvdz				
Bidentate	104.251	109.081	95.027	115.945
Tridentate	106.234	-	78.632	-
B3LYP/aug-cc-pvdz				
Bidentate	104.221	108.993	95.867	120.274
Tridentate	Collapsed To Bidentate			
B3LYP/aug-cc-pvdz+d				
Bidentate	104.509	108.999	95.027	115.945
Tridentate	106.224	-	79.769	-
B3LYP/cc-pvtz				
Bidentate	104.704	108.588	96.359	120.721
Tridentate	106.173	-	79.769	-
B3LYP/aug- cc-pvtz				
Bidentate	104.493	108.769	96.707	119.234
Tridentate	106.027	-	79.983	-

Table A-14: Bond Angles (in °) for $[Na(ClO_3)_2]^-$ isomers using the B3LYP functional and Dunning correlation consistent basis sets

Basis Set *Conformation*	**Uncorr.**	**ZPEC**	**ZPE**	**ΔE (kcal/mol)**
B3LYP/cc-pvdz				
Bidentate	-1533.7571	0.0197	-1533.7348	0
Tridentate	-1533.7631	0.0211	-1533.7420	+4.5181
B3LYP/aug-cc-pvdz				
Bidentate	-1533.8513	0.0204	-1533.8310	0
Tridentate	Collapsed To Bidentate			
B3LYP/aug-cc-pvdz+d				
Bidentate	-1533.9167	0.0215	-1533.8952	0
Tridentate	-1533.9076	0.0203	-1533.8874	+4.8946
B3LYP/cc-pvtz				
Bidentate	-1534.0462	0.0222	-1534.0240	0

Tridentate	-1534.0393	0.0212	-1534.0182	+3.6396
B3LYP/aug- cc-pvtz				
Bidentate	-1534.0627	0.0218	-1534.0408	0
Tridentate	-1534.0546	0.0208	-1534.0338	+4.3926

Table A-15: Energies for $[Na(ClO_3)_2]^-$ isomers using the B3LYP functional and Dunning correlation consistent basis sets

Basis Set *Conformation*	**Cl-O_u**	**Cl-O_b**	**M-O**	**M-Cl**
B3LYP/cc-pvdz				
Bidentate	Collapsed To Tridentate			
Tridentate	-	1.556	2.845	3.029
B3LYP/aug-cc-pvdz				
Bidentate	1.541	1.574	2.708	3.344
Tridentate	-	1.563	2.918	3.123
B3LYP/aug-cc-pvdz+d				
Bidentate	1.505	1.537	2.700	3.330
Tridentate	-	1.519	2.917	3.123
B3LYP/cc-pvtz				
Bidentate	1.495	1.526	2.703	3.292
Tridentate	-	1.516	2.895	3.099
B3LYP/aug- cc-pvtz				
Bidentate	1.497	1.528	2.706	3.339
Tridentate	-	1.516	2.909	3.120

Table A-16: Bond Lengths (in Å) for $[K(ClO_3)_2]^-$ isomers using the B3LYP functional and Dunning correlation consistent basis sets

Basis Set *Conformation*	**O_b-Cl-O_b**	**O_u-Cl-O_b**	**Cl-O_b-M**	**O_u-Cl-M**
B3LYP/cc-pvdz				
Bidentate	Collapsed To Tridentate			
Tridentate	107.005	-	81.321	-
B3LYP/aug-cc-pvdz				
Bidentate	105.693	108.538	99.287	116.337
Tridentate	106.654	-	82.418	-
B3LYP/aug-cc-pvdz+d				
Bidentate	105.823	108.618	99.974	118.589
Tridentate	106.864	-	83.083	-
B3LYP/cc-pvtz				
Bidentate	105.996	108.102	98.383	106.812
Tridentate	106.801	-	82.978	-
B3LYP/aug- cc-pvtz				
Bidentate	105.653	108.331	100.356	118.646
Tridentate	106.635	-	83.335	-

Table A-17: Bond Angles (in °) for $[K(ClO_3)_2]^-$ isomers using the B3LYP functional and Dunning correlation consistent basis sets

Basis Set *Conformation*	**Uncorr.**	**ZPEC**	**ZPE**	**ΔE (kcal/mol)**
B3LYP/cc-pvdz				
Bidentate	Collapsed To Tridentate			
Tridentate	-1971.3475	0.0201	-1971.3774	0
B3LYP/aug-cc-pvdz				
Bidentate	-1971.4839	0.0196	-1971.4643	0
Tridentate	-1971.4835	0.0193	-1971.4641	+0.1255
B3LYP/aug-cc-pvdz+d				
Bidentate	-1971.5490	0.0208	-1971.5282	+75.5401
Tridentate	-1971.6645	0.0207	-1971.6438	0
B3LYP/cc-pvtz				
Bidentate	-1971.6691	0.0215	-1971.6476	+1.0668
Tridentate	-1971.6706	0.0213	-1971.6493	0
B3LYP/aug- cc-pvtz				

Bidentate	-1971.6897	0.0211	-1971.6686	0
Tridentate	-1971.6761	0.0210	-1971.6551	+8.4714

Table A-18: Energies for $[K(ClO_3)_2]^-$ isomers using the B3LYP functional and Dunning correlation consistent basis sets

Method *Conformation*	**Cl-O_u**	**Cl-O_b**	**M-O**	**M-Cl**
PBEPBE/6-311+G(3df)				
Bidentate	1.489	1.527	2.352	2.945
Tridentate	-	1.513	2.588	2.756
B3LYP/6-311+G(3df)				
Bidentate	1.473	1.510	2.342	2.936
Tridentate	-	1.496	2.577	2.750
B3PW91/6-311+G(3df)				
Bidentate	1.465	1.499	2.349	2.941
Tridentate	-	1.487	2.583	2.757
HF/6-311+G(3df)				
Bidentate	1.428	1.468	2.340	2.925
Tridentate	-	1.513	2.587	2.757
LDA/6-311+G(3df)				
Bidentate	1.466	1.501	2.278	2.863
Tridentate	-	1.489	2.497	2.664
MPWPW91/6-311+G(3df)				
Bidentate	1.460	1.493	2.340	2.929
Tridentate	-	1.481	2.570	2.745

Table A-19: Bond Lengths (in Å) for $[Na(ClO_3)_2]^-$ isomers using the 6-311+G(3df) basis set and different functionals

Method *Conformation*	**O_b-Cl-O_b**	**O_u-Cl-O_b**	**Cl-O_b-M**	**O_u-Cl-M**
PBEPBE/6-311+G(3df)				
Bidentate	104.908	108.706	96.527	119.730
Tridentate	106.329	-	79.755	-

B3LYP/6-311+G(3df)				
Bidentate	104.605	108.639	96.983	119.495
Tridentate	106.169	-	80.183	-
B3PW91/6-311+G(3df)				
Bidentate	104.765	108.572	97.193	119.072
Tridentate	106.248	-	80.410	-
HF/6-311+G(3df)				
Bidentate	104.681	108.560	98.045	118.742
Tridentate	106.279	-	79.827	-
LDA/6-311+G(3df)				
Bidentate	104.534	108.385	96.323	119.874
Tridentate	105.930	-	79.507	-
MPWPW91/6-311+G(3df)				
Bidentate	104.747	108.531	97.218	119.044
Tridentate	106.174	-	80.419	-

Table A-20: Bond Angles (in °) for $[Na(ClO_3)_2]^-$ isomers using the 6-311+G(3df) basis set and different functionals

Method *Conformation*	**Uncorr.**	**ZPEC**	**ZPE**	**ΔE (kcal/mol)**
PBEPBE/6-311+G(3df)				
Bidentate	-1533.1460	0.0218	-1533.1242	0
Tridentate	-1533.1403	0.0211	-1533.1192	+3.1375
B3LYP/6-311+G(3df)				
Bidentate	-1534.0674	0.0227	-1534.0447	0
Tridentate	-1534.0599	0.0217	-1534.0381	+4.1416
B3PW91/6-311+G(3df)				
Bidentate	-1533.7404	0.0233	-1533.7171	0
Tridentate	-1533.7342	0.0225	-1533.7117	+3.3886
HF/6-311+G(3df)				
Bidentate	-1529.8982	0.0264	-1529.8718	0
Tridentate	-1529.8680	0.0229	-1529.8451	+16.7545
LDA/6-311+G(3df)				
Bidentate	-1529.0618	0.0233	-1529.0385	0
Tridentate	-1529.0559	0.0226	-1529.0333	+3.2630
MPWPW91/6-311+G(3df)				

Bidentate	-1533.9394	0.0238	-1533.9156	0
Tridentate	-1533.9333	0.0230	-1533.9102	+3.3886

Table A-21: Energies for $[Na(ClO_3)_2]^-$ isomers using the 6-311+G(3df) basis set and different functionals

Method *Conformation*	**Cl-O_u**	**Cl-O_b**	**M-O**	**M-Cl**
PBEPBE/6-311+G(3df)				
Bidentate	1.492	1.524	2.697	3.323
Tridentate	-	1.514	2.899	3.104
B3LYP/6-311+G(3df)				
Bidentate	1.476	1.507	2.701	3.326
Tridentate	-	1.497	2.906	3.117
B3PW91/6-311+G(3df)				
Bidentate	1.468	1.497	2.695	3.315
Tridentate	-	1.487	2.896	3.106
HF/6-311+G(3df)				
Bidentate	1.432	1.455	2.732	3.344
Tridentate	-	1.448	2.926	3.143
LDA/6-311+G(3df)				
Bidentate	1.467	1.499	2.587	3.202
Tridentate	-	1.489	2.778	2.978
MPWPW91/6-311+G(3df)				
Bidentate	1.463	1.490	2.687	3.092
Tridentate	-	1.482	2.883	3.092

Table A-22: Bond Lengths (in Å) for $[K(ClO_3)_2]^-$ isomers using the 6-311+G(3df) basis set and different functionals

Method *Conformation*	**O_b-Cl-O_b**	**O_u-Cl-O_b**	**Cl-O_b-M**	**O_u-Cl-M**
PBEPBE/6-311+G(3df)				
Bidentate	105.986	108.352	100.131	119.185
Tridentate	106.840	-	83.302	-
B3LYP/6-311+G(3df)				

Bidentate	105.732	108.315	100.610	117.839
Tridentate	106.722	-	823.589	-
B3PW91/6-311+G(3df)				
Bidentate	105.802	108.267	100.637	117.004
Tridentate	106.755	-	83.648	-
HF/6-311+G(3df)				
Bidentate	105.748	108.256	101.653	115.057
Tridentate	106.775	-	84.747	-
LDA/6-311+G(3df)				
Bidentate	105.591	108.068	99.731	121.269
Tridentate	106.452	-	82.622	-
MPWPW91/6-311+G(3df)				
Bidentate	105.798	108.216	100.619	116.377
Tridentate	106.718	-	83.652	-

Table A-23: Bond Angles (in °) for $[K(ClO_3)_2]^-$ isomers using the 6-311+G(3df) basis set and different functional

Method *Conformation*	**Uncorr.**	**ZPEC**	**ZPE**	**ΔE (kcal/mol)**
PBEPBE/6-311+G(3df)				
Bidentate	-1970.6791	0.0211	-1970.6581	+0.3765
Tridentate	-1970.6796	0.0209	-1970.6587	0
B3LYP/6-311+G(3df)				
Bidentate	-1971.7028	0.0220	-1971.6808	0
Tridentate	-1971.7023	0.0217	-1971.6805	+0.1883
B3PW91/6-311+G(3df)				
Bidentate	-1971.3637	0.0227	-1971.3410	+0.1883
Tridentate	-1971.3638	0.0224	-1971.3413	0
HF/6-311+G(3df)				
Bidentate	-1967.1968	0.0256	-1967.1712	0
Tridentate	-1967.1965	0.0253	-1971.1712	0
LDA/6-311+G(3df)				
Bidentate	-1965.9834	0.0227	-1965.9607	+0.5020
Tridentate	-1965.9839	0.0224	-1965.9615	0
MPWPW91/6-311+G(3df)				

Bidentate	-1971.6111	0.0231	-1971.5880	+0.3138
Tridentate	-1971.6114	0.0229	-1971.5885	0

Table A-24: Energies for $[K(ClO_3)_2]^-$ isomers using the 6-311+G(3df) basis set and different functionals